Morassi, A., Soler, A. & Zaera, R. (2017, septiembre). A continuum membrane model for small deformations of a spider orb-web. Mechanical Systems and Signal Processing, 93, 610-633.

DOI: 10.1016/j.ymssp.2017.02.018

A continuum membrane model for small deformations of a spider orb-web

Antonino Morassi*, Alejandro Soler† and Ramón Zaera‡

February 13, 2017

*Corresponding author. Polytechnic Department of Engineering and Architecture, University of Udine, via Cotonificio 114, 33100 Udine, Italy. Tel.: +39 0432 558739; fax: +39 0432 558700. E-mail: antonino.morassi@uniud.it

†Department of Continuum Mechanics and Structural Analysis, Universidad Carlos III de Madrid, Avda. de la Universidad 30, 28911 Leganés, Madrid, Spain. E-mail: asoler@ing.uc3m.es

‡Department of Continuum Mechanics and Structural Analysis, Universidad Carlos III de Madrid, Avda. de la Universidad 30, 28911 Leganés, Madrid, Spain. E-mail: rzaera@ing.uc3m.es

Abstract

In this paper we propose a continuum membrane model for the infinitesimal deformation of a spider web. The model is derived in the simple context of axially-symmetric webs formed by radial threads connected with circumferential threads belonging to concentric circles. Under suitable assumption on the tensile pre-stress acting in the referential configuration, the out-of-plane static equilibrium and the free transverse and in-plane vibration of a supported circular orb-web are studied in detail. The accuracy of the model in describing a discrete spider web is numerically investigated.

Keywords: System modelling; spider orb-webs; continuous structured membranes; small vibrations.

1 Introduction

The spider orb-web is a complex biological-mechanical system that has attracted increasing interest in the scientific literature in the last four decades. This web is a natural, lightweight, elegant structure with an extreme strength to weight ratio that is rarely observed among other structures, either natural or manmade. Its primary functions are for catching prey and sensory information, and the study of the mechanisms guiding the spider in prey capture and gathering information through web vibration has been - and actually is - one of the main objectives of the

research in this field. Interspecific and intraspecific variations in the structure of orb-webs is widely documented [1, 2, 3]. Moreover, individual spiders adapt the characteristics of the web to specific conditions such as nutritional status, spider size, presence of parasites or predators, type of prey available, weather conditions, or nutritional status [4]. Integrating both biological and biomechanical approaches can help to uncover how web architecture suits for vibratory sensing and prey catching under different circumstances, and to identify selective pressures that have guided their evolution. Basic questions posed by the researchers mainly concern: (i) how spiders might discriminate between the large set of web-borne vibrations and, particularly, between prey-produced signals and irrelevant vibrations such as those generated by wind; and (ii) how exactly the spider adjusts the web mechanics to the environmental conditions where the web is built, such as, the pre-stress tensile forces to be assigned at specific locations of the web, in order to improve its ability to prey capture. The answers to both questions fall on the understanding of the different physiological/behavioural processes. The use of modelling approaches could help to uncover the consequences behind the biological adaptations and evolutionary success of spiders.

In a series of papers published in the 80's, Master and co-authors studied, both experimentally and analytically, the vibration transmission through the web. Signal amplitude was very low and simplified linear dynamic models were used for the interpretation of the experiments. In [5] and [6] it was assumed that the radial strands are the most important vibration-conducting elements of the web. Accordingly, the types of

vibrations propagating through the web were classified into longitudinal, in-plane lateral and out-of-plane transverse. The conclusion was that, in an empty web, longitudinal vibration is almost not attenuated and, then, it plays a dominant role in the spider's choice of the path to reach the trapped prey. From the experiments emerged that the presence of a spider at the hub of the web induces a significant attenuation of the longitudinal vibration, and Masters [7] concluded that for prey detection and recognition all types of vibrations may be equally important. The first analytical estimates of resonant frequencies of spider orb-webs are due to Frolich and Buskirk [8]. The authors used simple mechanical models with lumped masses connected to crossing stretched threads. Landolfa and Barth [9] used in their experiments transmission of natural and artificial vibrations in webs to determine how spiders discriminate and locate the stimuli. Using a multidisciplinary approach, Mortimer et al. [10] studied vibrations in spider silks in comparison with other materials, identifying evolutionary trade-offs between mechanical and signalling functions. All the above analyses were strongly based on the one-dimensional character of the wave propagation through the web, even if it was more or less explicitly recognized in the literature the need of developing a vibration analysis of the web described as a two-dimensional sheet of threads.

In parallel to investigations on signal transmissions on the web, there has been an enormous increasing of research on bio-mechanical aspects of spider orb-webs [2]. Vollrath et al. [11] investigated on the effect of environmental and physiological variables, such as web support, wind, temperature, humidity and silk supply, on web geometry [12]. Wirth and Barth [13]

presented the first in situ measurement of the pre-stress forces in individual threads of intact spider webs, and provided arguments supporting the hypothesis of tension control by the spider. Gosline et al. [14] highlighted the influence of the dissipative behavior of the silk in the energy absorption capacity of the web, as compared to other constitutive behaviors. The effect of increases in thread tension on prey-detection efficiency was examined by Nakata [15]. Concerning the progress on the study of mechanical characterization of the spider silk, the experiments carried out by Ko and Jovicic [16] showed, among other aspects, that spider silk has toughness properties significantly higher than that of the strongest man-made fibers in tension, see also Harmer et al. [4]. The experiments and simulations performed by Cranford et al. [17] allowed to identify the nonlinear response of silk threads, and confirmed the superior resistance to structural defects (i.e., broken threads) in the spider web compared to other linear elastic or elasto-plastic materials. Hesselberg and Vollrath [18] investigated the mechanical behavior of the non-sticky permanent spiral in Nephila webs and, in particular, on the stress assigned by the spider to this spiral during web building.

Upon reviewing the literature it emerges that several issues of the two main questions i) and ii) posed at the beginning of this Introduction are still open. One of the reasons is probably connected with the lack of analytical/numerical studies on the mechanical behavior of the spider web as whole two-dimensional structure. The recent development of highly sophisticated numerical models of spider webs has partially overcome this limitation. Finite element analysis and numerical methods have been

identified and used by different authors as a valuable tool to integrate detailed data on web structure and silk properties, allowing to understand how silk biomechanics and web architectures interacted to influence spider web evolution along different structural pathways
[19, 16, 20, 23, 4, 21, 22, 17, 26, 27, 28]. For example, the effect of damage on the static and dynamic response of a web was numerically investigated by Ko and Jovicic [16] and Alam et al. [23]; an analysis of high performance spider silk was presented by Cranford et al. [17], Pugno et al. [24], Qin et al. [25]; the role of aerodynamic drag in the dissipation of prey's energy and in reducing deterioration of the orb web was considered by Zaera et al. [26]; the key effect of the secondary frame in avoiding excessive stiffness in radials was analysed by Soler and Zaera [27]; links between silk material properties and propagation of vibrations within webs were studied in Mortimer et al. [28]. These models offer a remarkable versatility and accuracy in reproducing the response of the web under wind loads, prey impacts or vibratory excitation. However, theoretical models often permit a deeper insight in the physical phenomena through the analysis of the underlying mathematical structure of the governing equations, which can be also written in nondimensional form to identify the most relevant parameters that rule the response of the web. The first two-dimensional model of spider web was proposed by Aoyanagi and Okumura [29, 30]. The model consists of radial and circumferential threads, and each thread is described as a stretched spring subject to pre-stress tensile force in the referential configuration. The model was used to determine the pre-stress state in an intact axially-symmetric web, and in a

web damaged by removing some circumferential threads. For the intact web, an infinitesimal homogeneous radial deformation was assigned from the unstressed state, and an analytical solution was provided. An approximate solution was proposed in case of damaged web. Numerical simulations showed that when radial threads are sufficiently strong compared to the circumferential threads, the damaged web is free of stress concentration, in contrast with what occurs in common materials. The model by Aoyanagi and Okumura was purely static, and its possible use for the study of either in-plane or out-of-plane response was not investigated, not even under the hypothesis of small deformations of the web.

In this paper we present a continuous mechanical model for small deformations of a spider orb-web. The actual discrete web, formed by a finite number of radial and circumferential threads, is approximated by a continuous elastic membrane on the assumption that the spacing between threads is small enough. The continuous membrane has a specific fibrous structure which is inherited from the original discrete web, and it is subject to tensile pre-stress in the referential configuration. Although the model can be adapted to reproduce general geometries, for simplicity here we restrict the attention to circular-shaped webs in which the circumferential threads belong to concentric circles. Furthermore, we study in detail the static and dynamic response of the web supported at the external boundary.

Our derivation of the continuum model follows a direct approach, namely, it is based on some a priori assumptions on the possible deformation of the membrane and on the internal contact forces acting in the radial and circumferential threads, see Tottenham and Williams [31] for a study of a

cable net in large-deflection membrane theory. For the sake of completeness, it should be recalled that important contributions to the understanding of the mechanical behavior of nets formed by cords have been done in the past, starting from the classical works by Rivlin and Pipkin (see, among others, the papers by Rivlin [32] and Pipkin [33]) to more recent results, see, for example, [34]. Much of the theory and nearly all of the applications developed in this area have been concerned with plane deformations of bodies reinforced throughout with two families of initially *parallel*, but not necessarily straight, fibers; we refer to Davini and Governatori [35] for a study of nets with hexagonal cell structure. The spider orb-web does not fall within this class of nets, since the geometrical structure naturally provides for an intensification of the density of radial threads towards the center of the web. In particular, a singularity in the model arises exactly at the center of the web (e.g., a stiffness coefficient diverges at that point), and this peculiar feature characterizes the static and dynamic behavior of the whole structure.

The paper is organized as follows. The mechanical model is derived in Section 2, and it is applied in Section 3 and Section 4 to describe the out-of-plane static equilibrium and the transverse free vibrations, respectively. Section 5 is devoted to the in-plane mechanical behavior of the web. A numerical study on the static and dynamic response of the model, and a comparison with a discrete web model are presented and discussed in Section 6 and 7. Section 8 presents the main outcomes of this work.

2 The mechanical model

2.1 Kinematics

We consider a spider web as a network formed by two intersecting families of threads which, in a referential configuration $\mathcal{B}_{\mathcal{K}}$, coincide with radial directions passing through the origin O of a two-dimensional Cartesian coordinate system (radial threads), and with coaxial circles centered at O (circumferential threads) and having radius ranging from 0 to R.
The threads of each family are supposed to be close enough to each other so that the web can be treated as a two-dimensional continuous membrane.
We define every material line tangent either to the radial or to the circumferential threads as radial fibre and circumferential fibre, respectively.
Moreover, we assume that during deformation no slippage occurs between fibers of the two different families, so that each given particle has the same two fibres passing through it at each stage of the deformation.
Let us denote by $\mathbf{X}$ the referential placement of the particle X in $\mathcal{B}_{\mathcal{K}}$. With reference to polar coordinate representation (see Figure 1), we have

$$\mathbf{X} = \mathbf{X}(\vartheta_1, \vartheta_2) = \vartheta_1(\cos\vartheta_2\mathbf{E}_1 + \sin\vartheta_2\mathbf{E}_2), \tag{1}$$

$$\vartheta_1 = \rho, \quad \vartheta_2 = \vartheta, \quad \vartheta_1 \in [0, R], \quad \vartheta_2 \in [0, 2\pi], \tag{2}$$

where $\{\mathbf{E}_1, \mathbf{E}_2, \mathbf{E}_1 \times \mathbf{E}_2 = \mathbf{E}_3\}$ is the canonical basis of $\mathbb{R}^3$, that is $\mathbf{E}_i \cdot \mathbf{E}_j = \delta_{ij}$, where $\delta_{ij} = 0$ if $i \neq j$ and $\delta_{ij} = 1$ if $i = j$, $i, j = 1, 2, 3$. Here, "$\times$" and "$\cdot$" denote the vector and scalar product in $\mathbb{R}^3$, respectively. The two families of continuous threads coincide with the coordinate curves $\vartheta_\alpha = const$, $\alpha = 1, 2$, on the reference configuration $\mathcal{B}_{\mathcal{K}}$. The unit tangent vector to the threads of the αth family is $\frac{\mathbf{A}_\alpha}{|\mathbf{A}_\alpha|}$, where $\mathbf{A}_\alpha = \mathbf{X}_{,\alpha}$, $\alpha = 1, 2$.

Here, $\{\mathbf{A}_1, \mathbf{A}_2, \mathbf{A}_3 = \frac{\mathbf{A}_1 \times \mathbf{A}_2}{|\mathbf{A}_1 \times \mathbf{A}_2|}\}$ is the covariant basis in a point $\mathbf{X}$ and $\{\mathbf{A}^1, \mathbf{A}^2, \mathbf{A}^3 = \mathbf{A}_3\}$ is the contravariant basis at the same point, with $\mathbf{A}^\alpha \cdot \mathbf{A}_\beta = \delta^\alpha_\beta$, where $\delta^\alpha_\beta = 1$ if $\alpha = \beta$ and $\delta^\alpha_\beta = 0$ is $\alpha \neq \beta$, $\alpha, \beta = 1, 2$. The comma notation is used to indicate partial derivatives, i.e., $\mathbf{X}_{,\alpha} = \frac{\partial \mathbf{X}}{\partial \vartheta_\alpha}$, $\alpha = 1, 2$. Greek indices assume values of 1, 2, and summation of the index is explicitly indicated.

The theory is restricted to infinitesimal deformations from the referential configuration $\mathcal{B}_\mathcal{K}$. A typical particle $\mathbf{X} \in \mathcal{B}_\mathcal{K}$ moves to the actual placement $\mathbf{x} = \mathbf{X} + \mathbf{u}(\mathbf{X})$, where the displacement vector field is given by the smooth function $\mathbf{u} : \mathcal{B}_\mathcal{K} \to \mathbb{R}^3$ represented as

$$\mathbf{u} = \sum_{\alpha=1}^{2} u^\alpha \mathbf{A}_\alpha + u^3 \mathbf{A}_3, \tag{3}$$

in which u^α, $\alpha = 1, 2$, u^3 are the contravariant components of $\mathbf{u}$. The assumption of infinitesimal deformations is implemented by requiring

$$\max \left(\frac{|\mathbf{u}(\mathbf{X})|}{R} + |\frac{\partial \mathbf{u}(\mathbf{X})}{\partial \mathbf{X}}| \right) < \epsilon, \quad \mathbf{X} \in \mathcal{B}_\mathcal{K}, \tag{4}$$

where ϵ is a given number belonging to $(0, 1)$, and by neglecting all the quantities of order $O(\epsilon^\tau)$ with $\tau > 1$. We shall denote by $\frac{\mathbf{a}_\alpha}{|\mathbf{a}_\alpha|}$ the unit tangent vector to the threads of the αth family in the actual configuration $\mathcal{B}$ of the membrane, namely

$$\mathbf{a}_\alpha = \mathbf{x}_{,\alpha}\,, \quad \alpha = 1, 2. \tag{5}$$

2.2 Internal contact forces and static equilibrium

We postulate that the internal force on an element of section along a coordinate curve in the actual configuration $\mathcal{B}$ is a tensile force acting in the

tangent plane to the deformed surface and, specifically, that the internal force on the αth family of threads corresponds to a tensile force in the "direction" of the αth coordinate curve (i.e., parallel to $\frac{\mathbf{a}_\alpha}{|\mathbf{a}_\alpha|}$). We denote by

$$\mathbf{n}\left(\mathbf{x}, \frac{\mathbf{a}^\alpha}{|\mathbf{a}^\alpha|}\right) \tag{6}$$

the force per unit length acting on an arc of the actual surface $\mathcal{B}$ having unit normal $\frac{\mathbf{a}^\alpha}{|\mathbf{a}^\alpha|}$, $\alpha = 1, 2$. Hereinafter, the contravariant basis $\{\mathbf{a}^1, \mathbf{a}^2, \mathbf{a}^3\}$ in a point of $\mathcal{B}$ is defined as $\mathbf{a}^\alpha \cdot \mathbf{a}_\beta = \delta^\alpha_\beta$, $\mathbf{a}^3 = \mathbf{a}_3$, see Figure 2.
The external force field acting on the deformed membrane is given by

$$\mathbf{p} = \sum_{\alpha=1}^{2} p^\alpha \mathbf{a}_\alpha + p^3 \mathbf{a}_3, \tag{7}$$

where p^α, p^3 are assumed to be continuous functions of $\mathbf{x}$, $\alpha = 1, 2$. By the Cauchy's Lemma, for every unit vector ν belonging to the tangent plane to the surface $\mathcal{B}$ at $\mathbf{x}$, there exists a unique stress tensor field $\mathbf{N} = \mathbf{N}(\mathbf{x})$ such that

$$\mathbf{n}(\mathbf{x}, \nu) = \mathbf{N}(\mathbf{x})\nu, \tag{8}$$

where

$$\mathbf{N} = \sum_{\alpha=1}^{2} \mathbf{N}^\alpha \otimes \mathbf{a}_\alpha, \tag{9}$$

$$\mathbf{N}^\alpha = \mathbf{n}\left(\mathbf{x}, \frac{\mathbf{a}^\alpha}{|\mathbf{a}^\alpha|}\right)|\mathbf{a}^\alpha| \equiv \sum_{\beta=1}^{2} N^{\alpha\beta}\mathbf{a}_\beta, \quad \alpha = 1, 2. \tag{10}$$

In particular, on the arc element of surface having normal $\frac{\mathbf{a}^2}{|\mathbf{a}^2|}$ a force parallel to $\mathbf{a}_2$ is acting and, similarly, on the arc element of surface of normal $\frac{\mathbf{a}^1}{|\mathbf{a}^1|}$ a force parallel to $\mathbf{a}_1$ is acting. Then

$$\mathbf{n}\left(\mathbf{x}, \frac{\mathbf{a}^\alpha}{|\mathbf{a}^\alpha|}\right) = d_\alpha \mathbf{T}_\alpha, \quad \alpha = 1, 2, \tag{11}$$

where $\mathbf{T}_\alpha$ is the traction on a *single thread* belonging to the αth coordinate curve (force vector parallel to $\mathbf{a}_\alpha$), and d_α is the number of threads per unit length on the coordinate curve $\vartheta_\alpha = const$ with direction coinciding with the vector $\mathbf{a}_\alpha$ (i.e., $[d_\alpha] = \frac{\#\ threads}{unit\ length}$).

The threads have zero shear/bending rigidity and the magnitude of the force $\mathbf{T}_\alpha$ depends only on the elongation in the direction of the αth coordinate curve. More precisely, we assume

$$\mathbf{T}_\alpha = (\overline{T}_\alpha + \mathcal{A}_\alpha \sigma_\alpha)\frac{\mathbf{a}_\alpha}{|\mathbf{a}_\alpha|}, \quad \alpha = 1, 2, \tag{12}$$

where $\overline{T}_\alpha > 0$ is the tensile pre-stress force acting on the referential configuration $\mathcal{B}_\mathcal{K}$; $\mathcal{A}_\alpha$ is the area of the cross-section of a single thread belonging to the αth family; and σ_α is the normal stress caused by the deformation on the thread. By (10)–(12) we have

$$\mathbf{N}^\alpha = d_\alpha(\overline{T}_\alpha + \mathcal{A}_\alpha \sigma_\alpha)\frac{|\mathbf{a}^\alpha|}{|\mathbf{a}_\alpha|}\,\mathbf{a}_\alpha, \quad \alpha = 1, 2, \tag{13}$$

or, in controvariant components,

$$N^{11} = d_1(\overline{T}_1 + \mathcal{A}_1\sigma_1)\frac{|a^{11}|^{\frac{1}{2}}}{|a_{11}|^{\frac{1}{2}}}, \tag{14}$$

$$N^{22} = d_2(\overline{T}_2 + \mathcal{A}_2\sigma_2)\frac{|a^{22}|^{\frac{1}{2}}}{|a_{22}|^{\frac{1}{2}}}, \tag{15}$$

$$N^{12} = N^{21} = 0, \tag{16}$$

where $a^{\alpha\alpha} = \mathbf{a}^\alpha \cdot \mathbf{a}^\alpha$ and $a_{\alpha\alpha} = \mathbf{a}_\alpha \cdot \mathbf{a}_\alpha$, $\alpha = 1, 2$.

Under the assumption of elastic material, we have

$$\sigma_\alpha = E_\alpha \epsilon_\alpha, \quad \alpha = 1, 2, \tag{17}$$

where $E_\alpha > 0$ is the Young's modulus of the material and ϵ_α is the elongation measure of the threads belonging to the αth family. By the

assumption (3) on the displacement field and after neglecting higher order terms, the linearized version of ϵ_α is

$$\epsilon_\alpha = \frac{u_\alpha|_\alpha}{A_{\alpha\alpha}}, \quad \alpha = 1, 2, \tag{18}$$

where $A_{\alpha\alpha} = \mathbf{A}_\alpha \cdot \mathbf{A}_\alpha$ and the covariant derivative of the covariant component u_α with respect to ϑ_α has the expression

$$u_\alpha|_\alpha = u_{\alpha,\alpha} - \sum_{\delta=1}^{2} \overline{\Gamma}^{\delta}_{\alpha\alpha} u_\delta, \quad \alpha = 1, 2. \tag{19}$$

Hereinafter, we denote by $\overline{\Gamma}^{\delta}_{\alpha\beta}$ the Christoffel symbol defined on the referential configuration $\mathcal{B}_\mathcal{K}$, i.e., $\overline{\Gamma}^{\delta}_{\alpha\beta} = \mathbf{A}_{\alpha,\beta} \cdot \mathbf{A}^\delta$, for α, β, $\delta = 1, 2$. In particular, we have

$$u_1|_1 = u_{1,1}\,, \tag{20}$$

$$u_2|_2 = u_{2,2} + \rho u_1. \tag{21}$$

A direct calculation shows that the factors appearing on the right hand side of (14), (15) are given by

$$\frac{|a^{11}|^{\frac{1}{2}}}{|a_{11}|^{\frac{1}{2}}} = 1 - 2u^1{}_{,1}\ , \tag{22}$$

$$\frac{|a^{22}|^{\frac{1}{2}}}{|a_{22}|^{\frac{1}{2}}} = \frac{1}{\rho^2}\left(1 - 2\left(u^2{}_{,2} + \frac{u^1}{\rho}\right)\right). \tag{23}$$

Finally, the equations of equilibrium can be derived by writing the Euler-Cauchy balance force equation for any portion of the actual configuration $\mathcal{B}$, using Cauchy's Lemma (8) and applying the Divergence Theorem. Under the assumption of smooth tensor and vector fields, we have

$$\sum_{\alpha=1}^{2} N^{\gamma\alpha}|_\alpha + p^\gamma = 0, \quad \text{in } \mathcal{B}, \quad \gamma = 1, 2, \tag{24}$$

$$\sum_{\alpha,\beta=1}^{2} N^{\beta\alpha} b_{\beta\alpha} + p^3 = 0, \quad \text{in } \mathcal{B}, \tag{25}$$

where

$$N^{\gamma\alpha}|_{\alpha} = N^{\gamma\alpha}{}_{,\alpha} + \sum_{\delta=1}^{2} N^{\gamma\delta}\Gamma^{\alpha}_{\delta\alpha} + \sum_{\delta=1}^{2} N^{\delta\alpha}\Gamma^{\gamma}_{\delta\alpha}, \tag{26}$$

$$\Gamma^{\gamma}_{\alpha\beta} = \mathbf{a}_{\alpha,\beta} \cdot \mathbf{a}^{\gamma}, \tag{27}$$

$$b_{\beta\alpha} = \sum_{\gamma=1}^{2} b^{\gamma}_{\alpha} a_{\gamma\beta}, \quad a_{\gamma\beta} = \mathbf{a}_{\gamma} \cdot \mathbf{a}_{\beta}, \quad b^{\gamma}_{\alpha} = -\mathbf{a}_{3,\alpha} \cdot \mathbf{a}^{\gamma}. \tag{28}$$

2.3 Fiber densities

We assume that the radial threads in $\mathcal{B}_{\mathcal{K}}$ are equally spaced in the plane angle 2π, and we also assume that the circumferential threads are equally spaced along the radial direction. Then, denoting by $\overline{d}_1$, $\overline{d}_2$ the thread densities in $\mathcal{B}_{\mathcal{K}}$, we have

$$\overline{d}_1 = \frac{C_\rho}{\rho}, \tag{29}$$

$$\overline{d}_2 = C_\vartheta, \tag{30}$$

where the two positive constants C_ρ, C_ϑ are the number $\overline{\#}_\rho$ of radial threads per unit plane angle and the number $\overline{\#}_\vartheta$ of circumferential threads per unit length along the radial direction, respectively. With reference to Figure 3, the definition (29) guarantees that the number of threads crossing the two arcs A_1B_1 (of radius ρ_1) and A_2B_2 (of radius ρ_2) coincide, i.e.

$$\begin{aligned} \overline{\#}_\rho(A_1B_1) &= \overline{d}_1(A_1B_1) \cdot \rho_1\varphi = C_\rho\varphi, \\ \overline{\#}_\rho(A_2B_2) &= \overline{d}_2(A_2B_2) \cdot \rho_2\varphi = C_\rho\varphi. \end{aligned} \tag{31}$$

where the angle φ is expressed in radians.

The expression of the fiber densities d_1, d_2 in the actual configuration $\mathcal{B}$ can be obtained by postulating the conservation of the number of threads

crossing a material fiber lying on a coordinate curve in $\mathcal{B}_\mathcal{K}$ and those crossing its image after the deformation. Then, we have

$$d_1 = \overline{d}_1 \left(\frac{A_{22}}{a_{22}} \right)^{\frac{1}{2}}, \tag{32}$$

$$d_2 = \overline{d}_2 \left(\frac{A_{11}}{a_{11}} \right)^{\frac{1}{2}}, \tag{33}$$

and, within the approximation of infinitesimal deformations and recalling (29)–(30),

$$d_1 = \overline{d}_1 \left(1 - \left(u^2{}_{,2} + \frac{u^1}{\rho} \right) \right), \tag{34}$$

$$d_2 = \overline{d}_2 \left(1 - u^1{}_{,1} \right). \tag{35}$$

Finally, by inserting (34)–(35) in (14)–(15), and taking into account (17)–(23), we obtain the linearized constitutive equations of the membrane stresses:

$$N^{11} = \overline{d}_1 \overline{T}_1 - \overline{d}_1 \overline{T}_1 \left(2u^1{}_{,1} + u^2{}_{,2} + \frac{u^1}{\rho} \right) + \overline{d}_1 \mathcal{A}_1 E_1 u_{1,1} \ , \tag{36}$$

$$N^{22} = \frac{\overline{d}_2 \overline{T}_2}{\rho^2} - \frac{\overline{d}_2 \overline{T}_2}{\rho^2} \left(u^1{}_{,1} + 2u^2{}_{,2} + 2\frac{u^1}{\rho} \right) + \frac{\overline{d}_2 \mathcal{A}_2 E_2 (u_{2,2} + \rho u_1)}{\rho^4}. \tag{37}$$

2.4 Pre-stress state

For vanishing displacement field, expressions (36)–(37) reduce to the membrane pre-stress state acting on the referential configuration $\mathcal{B}_\mathcal{K}$:

$$\overline{N}^{11} = \overline{d}_1 \overline{T}_1, \tag{38}$$

$$\overline{N}^{22} = \frac{\overline{d}_2 \overline{T}_2}{\rho^2}, \quad (\overline{N}^{12} = \overline{N}^{21} = 0). \tag{39}$$

The pre-stress field $\overline{N}^{\alpha\beta}$ is self-equilibrated, that is

$$\begin{cases} \sum_{\alpha=1}^{2} \overline{N}^{\gamma\alpha}|_{\alpha} = 0, \quad \text{in } \mathcal{B}_{\mathcal{K}}, \quad (\gamma = 1, 2) & (40) \\ \sum_{\alpha,\beta=1}^{2} \overline{N}^{\beta\alpha}\overline{b}_{\beta\alpha} = 0, \quad \text{in } \mathcal{B}_{\mathcal{K}}, & (41) \end{cases}$$

where the numbers $\overline{b}_{\beta\alpha}$, $\alpha, \beta = 1, 2$, are the entries of the second fundamental form of the web surface evaluated in the referential configuration $\mathcal{B}_{\mathcal{K}}$. Since all the $\overline{b}_{\beta\alpha}$'s vanish in $\mathcal{B}_{\mathcal{K}}$, the equilibrium equation (41) is identically satisfied. Equations (40) become

$$\begin{cases} \overline{N}^{\rho\rho}{}_{,\rho} + \frac{1}{\rho}\overline{N}^{\rho\rho} - \rho\overline{N}^{\vartheta\vartheta} = 0, \quad \text{in } \mathcal{B}_{\mathcal{K}}, & (42) \\ \overline{N}^{\vartheta\vartheta}{}_{,\vartheta} = 0, \quad \text{in } \mathcal{B}_{\mathcal{K}}, & (43) \end{cases}$$

where we have denoted $\overline{N}^{\rho\rho} = \overline{N}^{11}$, $\overline{N}^{\vartheta\vartheta} = \overline{N}^{22}$. Let $\overline{T}_{\rho} = \overline{T}_{1}$, $\overline{T}_{\vartheta} = \overline{T}_{2}$ and set $(\cdot)_{,\rho} = \frac{\partial(\cdot)}{\partial\rho}$, $(\cdot)_{,\vartheta} = \frac{\partial(\cdot)}{\partial\vartheta}$. Equation (43) implies

$$\overline{T}_{\vartheta} = \overline{T}_{\vartheta}(\rho). \tag{44}$$

Replacing (44) in (42) we obtain

$$\overline{T}_{\rho,\rho} = \xi\overline{T}_{\vartheta}(\rho), \tag{45}$$

where

$$\xi = \frac{C_{\vartheta}}{C_{\rho}}. \tag{46}$$

Hereinafter, we assume that the radial pre-stress is given at the boundary of the web as

$$\overline{T}_{\rho}(R, \vartheta) = \sigma = constant > 0, \quad \vartheta \in [0, 2\pi], \tag{47}$$

where σ is the tensile force applied on a single radial thread. By the symmetry of $\mathcal{B}_{\mathcal{K}}$ we have

$$\overline{T}_{\rho} = \overline{T}_{\rho}(\rho) \tag{48}$$

and the equilibrium problem in the radial direction reduces to

$$\begin{cases} \overline{T}'_{\rho}(\rho) = \xi \overline{T}_{\vartheta}(\rho), \quad \rho \in (0, R), & (49) \\ \overline{T}_{\rho}(R) = \sigma, & (50) \end{cases}$$

where $\overline{T}'_{\rho}(\rho) = \frac{d\overline{T}_{\rho}(\rho)}{d\rho}$. Problem (49)–(50) is underdetermined, since it involves two unknown functions in a single differential equation.

In order to introduce suitable a priori assumptions on the initial pre-stress, it is convenient to briefly recall the main steps of the process followed by spiders in creating their webs. The early stage of orb web construction, when anchor, frame and initial radii are laid, does not follow a fixed behavioral pattern [36]. Rather, the spider reacts in a flexible manner to adapt to a highly variable environment until the scaffold threads, made of major ampullate silk, stay in place. The second stage is made relying on a fixed behavioural pattern: the spider adds an *auxiliary* - or preliminary - spiral. This configuration is called *unfinished web*. Subsequently, the spider starts adding the threads of the *catching* - or sticky - spiral while, at the same time, removes the auxiliary spiral. This last configuration is the *finished web*.

As observed by Wirth and Barth [13], the pre-stress forces acting in the unfinished web differ greatly from those in the finished web. In particular, the measurements made by these authors along the radii and in the auxiliary spiral of webs of *Araneus diadematus* before the spiders added the catching spiral support the hypothesis of proportionality between $\overline{T}_{\vartheta}$ and $\overline{T}_{\rho}$, namely

$$\overline{T}_{\vartheta}(\rho) = k\overline{T}_{\rho}(\rho), \quad k > 0 \text{ constant}. \tag{51}$$

In fact, by replacing (51) into (49)–(50), the traction on a *single* radial thread increases exponentially from the center to the boundary of the web,

namely

$$\overline{T}_{\rho}(\rho) = \widehat{T}\exp(k\xi\rho), \quad \rho \in [0, R], \tag{52}$$

where the radial pre-stress at the center of the web is given by

$$\widehat{T} = \sigma\exp(-k\xi R) > 0. \tag{53}$$

Equation (52) reproduces well the behavior of the radial pre-stress measured by Wirth and Barth [13] in the unfinished web.
After the removal of the auxiliary spiral, part of the internal tensile pre-stress is taken up by the catching spiral. Due to the high extensibility of the catching spiral relative to that of frame threads and radii, the tensile pre-stress forces remain small in the catching spiral of the finished web. Wirth and Barth [13] proposed an indirect method for estimating the pretensional forces in the catching spiral by repeated force measurements at the same segment of a radius before and after cutting a spiral thread. Taking into account of the lack of direct measurement both of the tensile spiral pre-stress and of the gradient radial tension, we shall assume uniform tensile pre-stress in the circumferential threads of the finished web, namely

$$\overline{T}_{\vartheta}(\rho) = \mathcal{T} = constant, \quad \rho \in [0, R]. \tag{54}$$

By (49)–(50) we obtain

$$\overline{T}_{\rho}(\rho) = \widehat{T} + \xi\mathcal{T}\rho, \tag{55}$$

where the radial pre-stress at the center of the web $\widehat{T}$ is assumed to satisfy the condition

$$\widehat{T} = \sigma - \xi\mathcal{T}R > 0. \tag{56}$$

In the following sections we shall consider the mechanical behavior of the web both under the pre-stress state defined by (51)–(53) (unfinished web) and by (54)–(56) (finished web).

3 Out-of-plane static equilibrium

By replacing the expressions (36)–(37) of N^{11}, N^{22} in equation (25), and after linearization, we obtain the partial differential equation (with u^3 replaced by w) governing the out-of-plane equilibrium of the membrane:

$$\frac{C_\rho}{\rho}\overline{T}_\rho w_{,\rho\rho} + C_\vartheta \frac{\overline{T}_\vartheta}{\rho^2}(w_{,\vartheta\vartheta} + \rho w_{,\rho}) + p^3 = 0, \quad (\vartheta, \rho) \in (0, 2\pi) \times (0, R). \quad (57)$$

In the sequel, we shall consider in detail the axially-symmetric load condition

$$p^3 = p(\rho), \quad p \in C^0([0, R]), \quad (58)$$

for a circular membrane of radius R supported at the boundary, i.e.,

$$w(R) = 0. \quad (59)$$

Looking for a solution $w = w(\rho)$ and using (45), we obtain the self-adjoint equation

$$(\overline{T}_\rho w')' = -\frac{p\rho}{C_\rho}, \quad \rho \in (0, R). \quad (60)$$

The boundary condition at $\rho = 0$ can be derived by imposing the balance of the out-of-plane component of forces acting on the portion of surface $\mathcal{B}$ obtained as deformation of the small disk D_ϵ in $\mathcal{B}_\mathcal{K}$ centered at the origin O and having radius ϵ. Taking the limit of the balance force equation as $\epsilon \to 0$, we obtain the homogeneous Neumann end condition

$$\widehat{T} w'(0) = 0. \quad (61)$$

Equation (60), together with end conditions (59) and (61), admits the closed-form solution

$$w(\rho) = \frac{1}{C_\rho} \int_\rho^R \frac{1}{\overline{\overline{T}}_\rho(s)} \left(\int_0^s tp(t)dt \right) ds. \tag{62}$$

It should be noticed that the boundary condition (61) continues to hold even for less regular axially-symmetric loads, such as square summable p, i.e., $\int_0^R p^2(\rho)d\rho < +\infty$.

We conclude the section by highlighting a characteristic feature of our mechanical model of spider orb-web, namely, the ability to sustain a transverse concentrated force acting at the center O of the membrane. To show this property, let us model the concentrated force as a two-dimensional Dirac's delta function supported at O and with intensity $-P$, i.e., $-P\delta(O)$. The distribution $-P\delta(O)$ can be obtained as limit (in a suitable sense, see [37] for details) of the family of axially-symmetric loads $p_\epsilon^3(\rho)$ given by

$$p_\epsilon^3(\rho) = \begin{cases} -\frac{P}{\pi\epsilon^2}, \quad \rho \in (0, \epsilon), & (63) \\ 0, \quad \rho \in (\epsilon, R). & (64) \end{cases}$$

Then, by imposing the equilibrium of the out-of-plane component of the forces acting on the image (under the deformation) of the small disk D_ϵ in $\mathcal{B}_\mathcal{K}$ centered at the origin O and with radius ϵ, and taking the limit as $\epsilon \to 0$, we obtain the non-homogeneous Neumann condition

$$2\pi C_\rho \widehat{T} w'(0) = -P. \tag{65}$$

Under the above assumptions on the coefficients, the transverse displacement of the membrane supported at the boundary $\rho = R$ and under the concentrated force at the origin is given by

$$w(\rho) = \begin{cases} \frac{P}{2\pi C_\rho k\xi\sigma}\left(\exp(k\xi(R-\rho))-1\right) & \text{(unfinished web)}, \quad (66) \\ \frac{P}{2\pi C_\rho \xi\mathcal{T}}\ln\left(\frac{\sigma}{\sigma+\xi\mathcal{T}(\rho-R)}\right) & \text{(finished web)}, \quad (67) \end{cases}$$

where $\rho \in [0, R]$. It is not difficult to see that the center of the web is the only point of the web able to sustain a transverse concentrated force.

4 Transverse free vibrations

In this section we shall investigate on the infinitesimal transverse free vibrations of the web. It can be shown that the equation governing the free, undamped transverse motion $u^3 = u^3(\rho, \vartheta, t)$, where t is the time variable, can be obtained by assuming the function p^3 in (57) coinciding with the surface density of the out-of-plane transverse inertia forces. Denoting by m_ρ and m_ϑ the (time-invariant) linear mass density of the radial and circumferential threads, respectively, we can argue as in Section 2.3 in order to obtain the expression of the surface mass density γ of the continuum model. It turns out that

$$\gamma = \frac{C_\rho}{\rho} m_\rho + C_\vartheta m_\vartheta. \quad (68)$$

For the sake of simplicity, we shall assume $m_\rho = constant$, $m_\vartheta = constant$ in the sequel. Then, the equation of motion is

$$\frac{C_\rho}{\rho}\overline{T}_\rho u^3{}_{,\rho\rho} + C_\vartheta \frac{\overline{T}_\vartheta}{\rho^2}(u^3{}_{,\vartheta\vartheta} + \rho u^3{}_{,\rho}) - \gamma(\rho) u^3{}_{,tt} = 0, \quad (\vartheta, \rho, t) \in (0, 2\pi)\times(0, R)\times(0, \infty). \quad (69)$$

Setting

$$u^3(\rho, \vartheta, t) = w(\rho, \vartheta) y(t), \quad (70)$$

we can separate the spatial variables (ρ, ϑ) from the time variable t, obtaining

$$y'' + \lambda y = 0, \quad t > 0, \tag{71}$$

and

$$\frac{C_\rho}{\rho}\overline{T}_\rho w_{,\rho\rho} + C_\vartheta \frac{\overline{T}_\vartheta}{\rho^2}(w_{,\vartheta\vartheta} + \rho w_{,\rho}) + \lambda\gamma(\rho)w = 0, \quad (\vartheta, \rho) \in (0, 2\pi) \times (0, R), \tag{72}$$

where $\lambda \in \mathbb{R}^+$ is the eigenvalue to be determined. Looking for a solution to (72) of the form

$$w(\rho, \vartheta) = u(\rho)\Theta(\vartheta), \tag{73}$$

we obtain two uncoupled second-order differential equations in the unknown functions $\Theta(\vartheta)$ and $u(\rho)$:

$$\Theta'' + \nu^2\Theta = 0, \quad \vartheta \in (0, 2\pi), \tag{74}$$

$$(\overline{T}_\rho u')' + \lambda(m_\rho + \xi m_\vartheta \rho)u = \frac{\nu^2}{\rho} g u, \quad \rho \in (0, R), \tag{75}$$

where the (strictly positive) function $g = g(\rho)$ is given by

$$g(\rho) = \begin{cases} k\xi\overline{T}_\rho \quad \text{(unfinished web)}, & (76) \\ \xi\mathcal{T} \quad \text{(finished web)}. & (77) \end{cases}$$

Since $w(\rho, \vartheta)$, and hence $\Theta(\vartheta)$, must be periodic function of ϑ with period 2π, it follows that $\Theta(\vartheta)$ is a non-trivial solution to the eigenvalue problem

$$\begin{cases} \Theta'' + \nu^2\Theta = 0, \quad \vartheta \in (0, 2\pi), & (78) \\ \Theta(0) = \Theta(2\pi), & (79) \\ \Theta'(0) = \Theta'(2\pi). & (80) \end{cases}$$

Then, there exists an infinite sequence of eigenpairs to (78)–(80), that is

$$\nu_n^2 = n^2, \quad \Theta_n(\vartheta) = A\cos(n\vartheta) + B\sin(n\vartheta), \quad n = 0, 1, 2, ... \tag{81}$$

If $\nu_0 = 0$, then $\Theta_0(\vartheta) = constant(\neq 0)$ and the corresponding eigenfunctions w are axially-symmetric functions in the variable ρ. In particular, for $n = 0$ the singular term in the right hand-side of equation (75) disappears and we have the classical Sturm-Liouville problem

$$\begin{cases} (\overline{T}_\rho u_0')' + \lambda_0(m_\rho + \xi m_\vartheta \rho)u_0 = 0, \quad \rho \in (0, R), & (82) \\ u_0(R) = 0, \quad \text{(supported end condition)} & (83) \\ u_0'(0) = 0. & (84) \end{cases}$$

The last condition at $\rho = 0$ follows from the axially-symmetry of the eigenfunction w and from the absence of concentrated transverse inertia force acting at the origin O (see also the last part of Section 3). Therefore, under our assumptions, the eigenvalue problem (82)–(84) has an infinite sequence of real simple eigenvalues

$$0 < \lambda_{0,1} < \lambda_{0,2} < ...., \quad \text{with} \quad \lim_{m\to\infty} \lambda_{0,m} = \infty, \tag{85}$$

and a corresponding infinite sequence of eigenfunctions $\{u_{0,m}(\rho)\}_{m=1}^{\infty}$, which form an Hilbertian basis of the space of admissible deformations of the web.

If $n \geq 1$ in (81), then a singular term occurs at $\rho = 0$ (see equation (75)). The strain energy stored during the transversal deformation $u = u(\rho)$ is (apart the factor $\frac{1}{2}$)

$$\mathcal{E}(u, u') = \int_0^R \overline{T}_\rho(\rho)(u')^2 d\rho + \int_0^R \frac{n^2}{\rho} g u^2 d\rho \tag{86}$$

and the second integral takes finite values only if the function u vanishes at $\rho = 0$. Therefore, the eigenvalue problem for $n \geq 1$ is

$$\begin{cases} (\overline{T}_\rho u')' + \lambda(m_\rho + \xi m_\vartheta \rho)u = \frac{n^2}{\rho} g u, \quad \rho \in (0, R), & (87) \\ u(0) = 0, & (88) \\ u(R) = 0. & (89) \end{cases}$$

In order to investigate on this singular Sturm-Liouville eigenvalue problem with Coulomb-like potential, it is convenient to reduce the problem to Sturm-Liouville canonical form. Without going into details, it can be shown that by applying two Sturm-Liouville transformations in sequence, first the equation (87) is reduced to the so-called "impedance form", and then to the "standard canonical form"

$$y''(x) + G^2 \lambda y(x) = (\widetilde{q}(x) + V(x))y(x), \quad x \in (0, 1), \tag{90}$$

where $G = \int_0^R \left(\frac{m_\rho + \xi m_\vartheta \rho}{\overline{T}_\rho(\rho)} \right)^{\frac{1}{2}} d\rho$, $\widetilde{q}$ is a regular function in $[0, 1]$ and the potential $V(x)$ contains the singularity, namely $|V(x)| \leq \frac{K}{x}$ in $[0, 1]$ for some positive constant K. At this stage, the results by Carlson [38] show that, for every $n \geq 1$, our eigenvalue problem (87)–(89) has an infinite countable sequence of eigenpairs. Asymptotic estimates of the eigenpairs are also provided in [38].

Once the eigenvalue problem associated to the transverse free vibrations is solved, the transverse forced vibration problem can be addressed by expanding the transverse motion on the basis of the eigenfunctions and, then, using standard modal analysis methods.

We conclude this section with a couple of remarks. The first one concerns with the possibility to include a concentrated mass M (i.e., a

two-dimensional Dirac's delta point mass) at the center O of the web in the analysis of the transverse free vibration problem. Arguing as in Section 2 (second part), it can be shown that the eigenpairs corresponding to index $n \geq 1$ are not affected by the point mass at $\rho = 0$, and continue to satisfy the eigenvalue problem (87)–(89). On the contrary, all the eigenpairs corresponding to $n = 0$ are sensitive to the point mass M at $\rho = 0$, and they are solutions of the eigenvalue problem (82)–(84) with the boundary condition (84) replaced by

$$2\pi C_\rho \widehat{T} u_0'(0) = -\lambda_0 M u_0(0). \tag{91}$$

Clearly, the addition of the point mass M decreases the eigenvalues, namely $\lambda_{0,m}(M) < \lambda_{0,m}(M = 0)$ for every $m \geq 1$. Finally, recalling that the mass of the spider is (even more than) three orders of magnitude greater of the total mass of the web and also neglecting the dimensions of the spider mass, the orb-web model carrying a point mass as described above can be used to approximate the free transverse vibration of the web with the spider located at the center of the orb-web. Within the limits of this approximation, it is interesting to notice that the spider located at the center turns out to be not affected (actually, slightly affected) by the vibrations associated to the principal modes corresponding to $n \geq 1$, since all of them vanish at $\rho = 0$. Therefore, only the contribution of the axially-symmetric principal modes (i.e., those corresponding to $n = 0$) can be appreciated by the spider when it is located at $\rho = 0$.

The second remark is related to the boundary condition at $\rho = R$. In the above analysis, a supported (Dirichlet) boundary condition has been assumed at $\rho = R$. Real conditions may be different and may involve a

complicated interaction between the external part of the web and the frame and mooring threads. As a first attempt to include a more realistic boundary condition in our model, we can assume that frame and mooring threads globally act as an elastic suspension system that contrasts the transverse motion of the web by means of a continuum set of linearly elastic transversal springs located at the external boundary. Assuming, as a first approximation, that all the springs share the same elastic stiffness μ (per unit length), $\mu = constant > 0$, it can be shown that the whole previous treatment continues to hold by simply replacing the Dirichlet boundary condition $u(R) = 0$ by the *elastically restrained* end condition

$$\sigma u'(R) + \mu u(R) = 0. \tag{92}$$

5 In-plane mechanical behavior

The mechanical response to transverse forces is probably the most significant type of response in a spider web. However, there are situations in which also the in-plane behavior can be activated by external stimuli. This occurs when, for example, the pressure exerted by the wind is not exactly perpendicular to the web surface, or when an oblique impact of a prey induces in-plane waves which travel along the thread's axis or perpendicularly to the thread axis and in the plane of the web. The present section is devoted to a brief description of the in-plane behavior of the web. The equations governing the in-plane static equilibrium are obtained by inserting the constitutive equations of the stresses N^{11}, N^{22} within the equilibrium equations (24), and taking into account that the pre-stress field

$\overline{N}^{\alpha\beta}$ satisfies the system (40). After neglecting high order terms and putting $u^\rho = u^1$, $u^\vartheta = u^2$, we have

$$\begin{cases} \frac{C_\rho}{\rho}\mathcal{A}_\rho E_\rho u^\rho{}_{,\rho\rho} - \frac{C_\vartheta}{\rho^2}\mathcal{A}_\vartheta E_\vartheta(\rho u^\vartheta{}_{,\vartheta} + u^\rho) + \\ + \frac{C_\vartheta}{\rho^2}\overline{T}_\vartheta(u^\rho{}_{,\vartheta\vartheta} - \rho u^\vartheta{}_{,\vartheta}) + p^\rho = 0, \\ \frac{C_\vartheta}{\rho^3}\mathcal{A}_\vartheta E_\vartheta(\rho u^\vartheta{}_{,\vartheta\vartheta} + u^\rho{}_{,\vartheta}) + \frac{C_\vartheta}{\rho^2}\overline{T}_\vartheta(\rho u^\vartheta{}_{,\rho} + \frac{1}{\rho}u^\rho{}_{,\vartheta}) + \qquad (93) \\ + \frac{C_\rho}{\rho}\overline{T}_\rho(u^\vartheta{}_{,\rho\rho} + \frac{2}{\rho}u^\vartheta{}_{,\rho}) + p^\vartheta = 0, \qquad (94) \end{cases}$$

for $(\vartheta, \rho) \in (0, 2\pi) \times (0, R)$. Hereinafter, we find convenient to introduce the notation $\mathcal{A}_\rho E_\rho = \mathcal{A}_1 E_1$, $\mathcal{A}_\vartheta E_\vartheta = \mathcal{A}_2 E_2$. Postponing the analysis of the solutions to the general problem (93)–(94) to future work, in the sequel we shall consider in detail a couple of special cases.

Case i). Axially-symmetric load. We consider the load

$$p^\rho = p^\rho(\rho) \in C^0([0, R]), \quad p^\vartheta \equiv 0 \tag{95}$$

acting on a circular membrane supported at the boundary. By symmetry, we look for a solution

$$u^\rho = u^\rho(\rho), \quad u^\vartheta \equiv 0. \tag{96}$$

Equation (94) is identically satisfied and equation (93) becomes

$$\mathcal{A}_\rho E_\rho (u^\rho)'' - \frac{\xi}{\rho}\mathcal{A}_\vartheta E_\vartheta u^\rho = -\frac{\rho p^\rho}{C_\rho}, \quad \rho \in (0, R), \tag{97}$$

with end conditions

$$u^\rho(0) = 0, \quad u^\rho(R) = 0. \tag{98}$$

Equations (97)–(98) describe the longitudinal deformation of a supported rod with axial stiffness $\mathcal{A}_\rho E_\rho$ resting on an elastic Winkler soil foundation with subgrade coefficient $\frac{\xi}{\rho}\mathcal{A}_\vartheta E_\vartheta$, and subject to a longitudinal force field

$\frac{\rho p^\rho}{C_\rho}$. One can show that there exists a unique solution $u^\rho \in C^2(0,R)$ to (97)–(98).

Case ii). Circumferential load. Let us assume

$$p^\rho \equiv 0, \quad p^\vartheta = p^\vartheta(\rho) \in C^0([0,R]) \tag{99}$$

and

$$u^\rho \equiv 0, \quad u^\vartheta = u^\vartheta(\rho). \tag{100}$$

Under the above assumptions, equation (93) is identically satisfied, whereas equation (94) can be written as

$$(u^\vartheta)'' = -f(\rho) - (u^\vartheta)' \left(\frac{\overline{T}'_\rho}{\overline{T}_\rho} + \frac{2}{\rho} \right), \quad \rho \in (0,R), \tag{101}$$

where

$$f(\rho) = \frac{\rho p^\vartheta}{C_\rho \overline{T}_\rho}. \tag{102}$$

To solve (101) it is convenient to introduce the covariant component u_ϑ of the circumferential displacement, which is related to the contravariant component as

$$u_\vartheta = u^\vartheta \rho^2. \tag{103}$$

Solving (101) with respect to u_ϑ and imposing the boundary conditions $u_\vartheta(0) = 0 = u_\vartheta(R)$, one can determine the closed-form expression

$$u_\vartheta(\rho) = \mathcal{G}(\rho) - \mathcal{G}(0) \cdot \frac{\ln\left(\frac{\overline{T}_\rho(\rho)}{\sigma}\right)}{\ln\left(\frac{\overline{T}_\rho(0)}{\sigma}\right)}, \tag{104}$$

where

$$\mathcal{G}(\rho) = -\int_R^\rho s^2 \left(\int_0^s \frac{t p^\vartheta(t)}{C_\rho \overline{T}_\rho(t)} dt \right) ds. \tag{105}$$

We conclude the section with the analysis of the axially-symmetric in-plane free vibration problem. By using the surface mass density γ as in (68) and assuming free vibrations, with radian frequency $\sqrt{\lambda}$, of the form

$$u^{\vartheta}(\rho,\vartheta,t)\equiv 0,\quad u^{\rho}(\rho,\vartheta,t)=u(\rho)\cos(\sqrt{\lambda}t), \tag{106}$$

the eigenvalue problem for $u=u(\rho)$ is

$$\begin{cases} \mathcal{A}_{\rho}E_{\rho}u''-\frac{\xi}{\rho}\mathcal{A}_{\vartheta}E_{\vartheta}u+\lambda(m_{\rho}+\xi m_{\vartheta}\rho)u=0, \quad \rho\in(0,R), & (107)\\ u(0)=0, & (108)\\ u(R)=0. & (109) \end{cases}$$

This problem is analogous to the Sturm-Liouville singular eigenvalue problem (87)–(89) governing the out-of-plane free vibrations of the membrane with $n\geq 1$. It should be noted that the eigenvalues of (107)–(109) are not influenced by the pre-stress state.

6 Numerical simulations

Goal of this section is two-fold. The first objective is concerned with estimating the solution of out-of-plane and in-plane free vibration of our two-dimensional membrane model via finite element solution. The second one refers to the ability of the continuous membrane model in predicting the statical and low-frequency dynamic response of a "real" discrete spider web.

6.1 Finite element solution of the continuous eigenvalue problem

In this section we present a finite element solution of the eigenvalue problem associated to the free transverse vibrations of the web. The results and numerical simulations refer to supported condition on the external boundary. Other type of boundary conditions, such as, for example, the concentrated mass at the center (91), or the elastically restrained boundary condition (92), can be analyzed analogously.

We first consider the problem (87)–(89) corresponding to $\nu_n = n^2$, with $n \geq 1$.

Let us denote by $H_0^1(0,R)$ the Hilbert space formed by the functions $f : (0,R) \to \mathbb{R}$ such that the H^1-norm of f is finite, i.e., $||f||_{H^1} = \left(\int_0^R (f^2 + (f')^2)\right)^{\frac{1}{2}} < \infty$, and the trace of f both at $\rho = 0$ and $\rho = R$ vanishes, i.e., $f(0) = f(R) = 0$. Here, f' is the weak derivative of f.

The weak formulation of (87)–(89) consists in determining a non-trivial function $u \in H_0^1(0,R)$ such that

$$a(u,\psi) = \lambda b(u,\psi), \quad \text{for every } \psi \in H_0^1(0,R), \tag{110}$$

where the real, symmetric, continuous bilinear forms $a(\cdot,\cdot) : H_0^1(0,R) \times H_0^1(0,R) \to \mathbb{R}$, $b(\cdot,\cdot) : H_0^1(0,R) \times H_0^1(0,R) \to \mathbb{R}$ are defined as

$$a(u,\psi) = \int_0^R \overline{T}_\rho u'\psi' d\rho + n^2 \int_0^R \frac{1}{\rho} g u \psi d\rho, \tag{111}$$

$$b(u,\psi) = \int_0^R (m_\rho + \xi m_\vartheta \rho) u \psi d\rho \tag{112}$$

and the function $g = g(\rho)$ is defined in (76)–(77). It should be recalled that the function g is identically equal to the positive constant $\xi\mathcal{T}$ in case of

finished web, and $g = k\xi\overline{T}_\rho$, $g \in C^2([0,R])$ and $g > 0$ in $[0,R]$, for the unfinished web.

To find a discrete version of (110), we look for an approximation of the eigenpair (λ, u) in the subspace $H^1_{0(J)}(0,R)$ of $H^1_0(0,R)$ formed by the linear combinations of the piecewise-linear spline functions $\{\psi_j(\rho)\}$ defined as

$$\psi_j(\rho) = \begin{cases} \frac{\rho-\rho_{j-1}}{\rho_j-\rho_{j-1}}, & \rho_{j-1} \le \rho \le \rho_j, \quad (113) \\ \frac{\rho_{j+1}-\rho}{\rho_{j+1}-\rho_j}, & \rho_j \le \rho \le \rho_{j+1}, \quad (114) \end{cases}$$

$j = 1, ..., J$, where $\rho_0 = 0 < \rho_1 < \rho_2 < ... < \rho_J < \rho_{J+1} = R$. Let

$$u_{(J)}(\rho) = \sum_{j=1}^{J} \widehat{u}_j \psi_j(\rho) \tag{115}$$

be the approximation of the eigenfunction u. Replacing (115) in (110) and taking $\psi = \psi_i$, $i = 1, ..., J$, the vector $\widehat{\mathbf{u}} = (\widehat{u}_1, ..., \widehat{u}_J) \in \mathbb{R}^J$ satisfies the J-dimensional eigenvalue problem

$$\mathbf{K}_{(J)}\widehat{\mathbf{u}} = \lambda_{(J)}\mathbf{M}_{(J)}\widehat{\mathbf{u}}, \tag{116}$$

where the (i,j)-entry of the stiffness and inertia matrices is given by

$$K_{(J)i,j} = a(\psi_i, \psi_j), \quad M_{(J)i,j} = b(\psi_i, \psi_j), \tag{117}$$

and $\lambda_{(J)}$ is an approximation of the eigenvalue λ. The solution of the algebraic eigenvalue problem (117) permits to determine an approximation of the eigenpairs of the continuum web model.

The analysis of both the axially-symmetric vibrations (82)–(84) with $\nu_0^2 = 0$ and the in-plane vibrations (problem (107)–(109)) can be carried out analogously. For the axially-symmetric case, in particular, it is enough to

replace the set of admissible deformations $H_0^1(0,R)$ with the larger set $H_{(R)}^1(0,R) = \{f : (0,R) \to \mathbb{R} |\ ||f||_{H^1} < \infty,\ f(R) = 0\}$.
In all cases, the number of intermediate nodes for the finite element solution of the continuous eigenvalue problem has been assumed equal to $J = 40$. This value is the minimum one permitting to satisfy a criterion for the convergence up to the 10th eigenfrequency (maximum eigenfrequency considered in the analysis), which guarantees that the incremental difference in the eigenfrequency values for an additional node would be lower than 1%.

6.2 Reference discrete model and equivalence with continuum model

Let us consider an axially-symmetric discrete web composed, in the reference configuration $\mathcal{B}_\mathcal{K}$, of n_ρ radial threads of length R, and n_ϑ regular polygons with n_ρ sides, see Figure 4. This reference geometry resembles the arrangement of radials and spirals in the capture area of the orb web. Radial threads are intersected by polygons at equal distances, leading to $n_\vartheta + 1$ segments of length $\Delta\rho = R/\left(n_\vartheta + 1\right)$. The angular distance between radials is $\Delta\vartheta = 2\pi/n_\rho$.
Let ϕ_ρ and ϕ_ϑ be the diameters of radial and circumferential threads, respectively. The geometric and inertial equivalence between the discrete web and its continuum counterpart, described in previous sections, is established through the following relations:

$$C_\vartheta = \tfrac{1}{\Delta\vartheta}, \tag{118}$$

$$C_\rho = \tfrac{1}{\Delta\rho}, \tag{119}$$

$$m_\rho = \pi \tfrac{\phi_\rho^2}{4} \varrho_S, \tag{120}$$

$$m_\vartheta = \pi \tfrac{\phi_\vartheta^2}{4} \varrho_S, \tag{121}$$

ϱ_S being the constant volume mass density of the silk. The selected geometrical and mechanical parameters of the web are shown in Table 1. Regarding the pre-stress field, equivalence between discrete and continuum models is established by imposing, in the reference configuration, the following tensile force in each radial segment i $(i = 1, ..., n_\vartheta + 1)$

$$\overline{T}_{\rho}^{\,i} = \widehat{T}\, \frac{\exp(k\xi\,(i-1)\,\Delta\rho) + \exp(k\xi i \Delta\rho)}{2} \tag{122}$$

for the exponential pre-stress profile, and

$$\overline{T}_{\rho}^{\,i} = \widehat{T} + \xi \mathcal{T} \Delta\rho \left(i - \frac{1}{2} \right) \tag{123}$$

for the linear radial pre-stress profile. Self-equilibrium at the joints between radial and circumferential threads is achieved by imposing the following tensile forces in all the segments of each polygon j $(j = 1, ..., n_\vartheta)$

$$\overline{T}_{\vartheta}^{\,j} = \frac{1}{2\sin\left(\Delta\vartheta/2\right)} \left(\overline{T}_{\rho}^{\,j+1} - \overline{T}_{\rho}^{\,j} \right). \tag{124}$$

The values of the geometric parameters have been selected aiming at reproducing the capture area of a web built by an *Araneus diadematus*, following the characteristic dimensions presented in [11], and in agreement with the models proposed by other authors, see, for example, [23] and [26]. The mass density of the silk threads ϱ_S was taken from [16], and the diameter of circumferential and radial threads from [26]. The parameters $\widehat{T}$,

and η or $\mathcal{T}$, defining the pre-stress state acting on the referential configuration, have been defined consistently with the experimental results provided by Wirth and Barth [13] for auxiliary and catching spirals. Table 2 shows the selected values of the above parameters.

The model has been implemented in the finite element code ABAQUS/Standard (version $6.14-2$) using linear truss elements for silk threads, with a characteristic element length equal to 0.45 mm. This permitted to evaluate natural frequencies, mode shapes, and quasi-static deformations of the discrete web.

7 Comparison between continuous and discrete models

7.1 Non-dimensional equations

The results obtained with discrete and continuum models will be presented and compared in nondimensional form. To that aim, we define the following nondimensional variables

$$\tilde{\rho} = \frac{\rho}{R}, \quad \tilde{u} = \frac{u}{R}, \quad \tilde{w} = \frac{w}{R}, \quad \widetilde{T}_\rho = \frac{\overline{T}_\rho}{\widehat{T}}, \tag{125}$$

and nondimensional parameters

$$\tilde{\xi} = \xi R, \quad \kappa = \frac{m_\vartheta}{m_\rho}, \quad \Upsilon = \frac{\mathcal{A}_\vartheta E_\vartheta}{\mathcal{A}_\rho E_\rho}, \quad \tilde{p} = \frac{pR^2}{\widehat{T}}, \quad \tilde{P} = \frac{P}{\widehat{T}}, \tag{126}$$

$$\chi = \frac{\xi R \mathcal{T}}{\widehat{T}}, \quad \tilde{k} = k\xi R, \tag{127}$$

permitting to derive nondimensional expressions for the governing equations or, if available, for their closed-form solutions.

The nondimensional version of equation (75), governing the transverse free vibration, is

$$(\widetilde{T}_\rho \tilde{u}')' + \Lambda_t \left(1 + \tilde{\xi}\kappa\tilde{\rho}\right) = \frac{\nu^2 R}{\widehat{T}\tilde{\rho}} g\tilde{u}, \qquad \tilde{\rho} \in (0,1), \tag{128}$$

where the nondimensional eigenvalue has the expression

$$\Lambda_t = \frac{R^2 m_\rho}{\widehat{T}}\lambda. \tag{129}$$

Then, the dimensional eigenfrequency ω and its nondimensional counterpart Ω are related by

$$\omega = \frac{1}{R}\sqrt{\frac{\widehat{T}}{m_\rho}}\ \Omega. \tag{130}$$

For the reference discrete model defined by the parameters in Tables 1–2, the factor multiplying Ω in equation (130) takes the value 303 Hz for the auxiliary spiral, and 906 Hz for the catching spiral.

Likewise, the nondimensional equation for in-plane free vibration (107) becomes

$$\tilde{u}'' + \Lambda_\rho \left(1 + \tilde{\xi}\kappa\tilde{\rho}\right) = \frac{\tilde{\xi}\Upsilon}{\tilde{\rho}}\tilde{u}, \qquad \tilde{\rho} \in (0,1), \tag{131}$$

where we identify by

$$\Lambda_\rho = \frac{R^2 m_\rho}{\mathcal{A}_\rho E_\rho}\lambda \tag{132}$$

the nondimensional eigenvalue stating the relation between dimensional, ω, and nondimensional, Ω, eigenfrequencies:

$$\omega = \frac{1}{R}\sqrt{\frac{\mathcal{A}_\rho E_\rho}{m_\rho}}\ \Omega. \tag{133}$$

For the reference discrete model, the factor multiplying Ω in equation (133) takes the value 26376 Hz and it does not depend on the pre-stress state.

7.2 Out-of-plane static equilibrium

The effect of a uniformly distributed load and of a point load concentrated at the origin, applied to the web either with auxiliary or catching spiral, has been evaluated using continuum and discrete models. The values of point and distributed loads considered in simulations are $\tilde{p} = 0.1$ and $\tilde{P} = 0.1$, which permitted to fulfill the hypothesis of small deformations due to their low magnitude.

Figures 5 and 6 show the comparison of transverse displacement along a radius, for webs with auxiliary and catching spirals, respectively. As it can be observed, the continuum model faithfully reproduces the deformation of the discrete web. It is worth noting that the average gradient of pre-stress along a radial thread is two orders of magnitude higher when the auxiliary spiral is present, as compared to the web with catching spiral, thus leading to a sharper increase in the deformation close to $\rho = 0$ when a concentrated point force is applied.

7.3 Transverse free vibrations

The unfinished web is characterized by low value of the pre-stress at the center and by high radial pre-stress gradient, leading to taut radial and circumferential threads in the whole web except in the close vicinity of the center. In the finished web, conversely, the tensile pre-stress in the circumferential threads keep at a fairly low (constant) value in the whole web, whereas radial threads attain high pre-stress value along their entire length. As reported below, these peculiarities of the pre-stress field are responsible of different transverse vibrational responses of the web.

Tables 3 and 4 show the first ten nondimensional frequencies corresponding to the free transverse vibration of the *unfinished* web, for $n = 0$ to $n = 3$. The relative error in the prediction of the continuum model is very low for the first modes, and keeps rather small value even for higher modes. Likewise, the mode shapes predicted by the discrete model are properly captured by the continuum model, as it can be seen from Figures 7 and 8. The accuracy of the continuum approach can be further seen in Figure 9, in which the transverse displacement $\tilde{u}(\tilde{\rho})$ of the first four modes of the family $n = 0$ is depicted.

A comparison between the values of the first low eigenfrequencies of the transverse vibrations of the *finished* web estimated by the continuous and discrete model is shown in Table 5. Differences are appreciable and starting from the fourth mode the discrepancy is more than 35% for some radial class $n = 0 - 3$. The corresponding mode shapes also deviate significantly, as it is shown in Figure 10 (radial direction) and in Figure 11 (three-dimensional views). This latter figure, in particular, shows that large transverse vibrations occur in the few external circumferential threads of the web, starting from the fourth mode of the discrete model.

A detailed inspection of Figure 11 shows that the transverse deformation of each external circumferential thread resembles to the fundamental mode shape of the thread under fixed supports. A possible explanation for this behavior, and for the appearance of vibration modes having local character, may be due to the proximity between the frequency of the fourth 'global' vibration mode of the discrete model ($\Omega = 1.044$, 1.092, 1.098, 1.107, for $n = 0, 1, 2, 3$, respectively) and the fundamental frequency of the external

circumferential thread between two contiguous radial threads ($\Omega = 1.129$). If the two natural frequencies were exactly equal, then any combination of the corresponding vibration modes would be an eigenfunction of the web. Actually, the two frequencies are very close, even if they do not exactly coincide, and therefore it is quite expectable that the global mode shape can be affected by the local character of the external circumferential thread's vibration. This behavior does not occur in the case of the auxiliary spiral, since the fundamental frequency of a single circumferential thread close to the boundary is much larger than the natural frequency of the global vibration modes belonging to this frequency range. It should be also noticed that these local effects on the vibration modes are gradually reduced as we move towards the center of the web, since the fundamental frequency of each circumferential thread between two successive radial threads moves away from the global frequency range.

The above mentioned local effects make the identification and classification of the eigenfunctions of the transverse vibrations of the finished web rather complicated, also because the eigenfunctions become more and more complex and wavy as the natural frequency increases. Following a common practice in other contexts of Structural Dynamics, it has been checked that the local behavior is considerably reduced if the mass of the circumferential wires is lumped at the thread intersections, that is, assigned to the degree of freedom of the node located at the joints between radial and spiral threads. As shown in Table 5 (sixth column) and in Figures 10 and 11, a very good agreement between the discrete model and the continuum model is obtained for the first four eigenpairs of the radial classes $n = 0 - 3$. It

should be remarked that the eigenfrequency error is less than 6.5% up to the first ten natural frequencies of the classes $n = 0 - 3$. For the sake of completeness, we also notice that the additional lumping of the mass of the radial threads does not produce appreciable changes in the eigenfrequency values and in corresponding eigenfunctions.

7.4 In-plane free vibrations

We conclude the comparison of results between discrete and continuous model by investigating the axially-symmetric in-plane free vibration of the finished web. It should be recalled that the corresponding eigenpairs are not influenced by the pre-stress state, but they depend on fiber densities. As shown in Table 6, the prediction of the eigenfrequencies by the continuum model is highly accurate and the error keeps below 5% even for the tenth mode. First four principal vibration modes are shown in Figure 12, revealing the ability of the continuum model to capture the dynamic in-plane deformation of the web.

8 Conclusions

The arrival of novel experimental and bio-modelling techniques has provoked a shift to the quantitative side in studies aiming at understanding biological systems, opening a doorway to a more complex and detailed reality. Specifically, models can help to uncover new phenomena, set up a framework for interpreting data, or guide experimental designs.
The principal goal of this work is to provide a continuum model for the

analysis of the mechanical behavior of spider orb-webs, suitable for small deformations, through which deeper insights can be gained. The model overcomes the limitations of previous theoretical approaches, by inheriting the fibrous structure of the discrete web. The governing equations have been derived using a direct approach based on appropriate assumptions on the internal contact forces. Webs built by spiders exhibit considerable interspecific in various aspects. Moreover, spiders alter details of individual webs in response to both their internal physiology and the external environment. Since the continuum model has been formulated in a general framework, one of its main characteristics is the possibility to describe the static and dynamic behavior of webs exhibiting a wide variability, as is the case with real spider webs. Thus, the stiffness and inertial properties of the silk, the density of radial and spiral threads, or the pre-tensile field, all of which are under control by the spider upon silk spun and web construction, can be modified in order to analyze their effect in both the static and the dynamic response.

The resulting partial differential equations are tractable and, assuming uniform properties of the radial and circumferential threads, have been solved for certain classes of static and dynamic problems. The accuracy of the continuous model in reproducing the mechanical response of a discrete orb-web has been tested by comparison with the results of the numerical model of a web composed of threads.

The model presented herein represents a first step in the development of a simulation tool for understanding the design of the orb web as a catching structure that also has sensory functions. The model is especially suited for

the analysis of the propagation of waves throughout the web and connections with the ability of the spider to locate and discriminate between subtle vibratory signals generated by prey, predators or mates. To that aim, applications of the present theory to topics of on-going research are the determination of the in-plane and out-of-plane dynamic response of the web under a generic load condition, and the study of the inverse problem consisting in determining the prestress state by measurements of the natural frequencies of the out-of-plane free motions of the web.

Acknowledgement

Part of this work has been developed during visits of A. Morassi to the Department of Continuum Mechanics and Structural Analysis of the Universidad Carlos III de Madrid in the years 2015 and 2016. A. Morassi wishes to thank the colleagues for the warm hospitality at UC3M. The authors of the Universidad Carlos III de Madrid are indebted to the Ministerio de Economía y Competitividad de España for financial support under grant DPI2014-57989-P.

References

[1] M.E. Herberstein, I.M. Tso, Spider webs: evolution, diversity and plasticity. In Spider behaviour: flexibility and versatility, M.E. Herberstein Ed., Cambridge University Press (2011) 57–85.

[2] T.A. Blackledge, M. Kutner, I. Agnarsson, The form and function of spider orb webs: evolution from silk to ecosystems. Advances in Insect Physiology 41 (2011) 175–262.

[3] C. Boutry, S.J. Blamires, Plasticity in spider webs and silk: an overview of current evidence. In Spiders: morphology, behavior and geographic distribution, M. Santerre Ed., Nova, New York (2013) 1–46.

[4] A.M.T. Harmer, T.A. Blackledge, J.S. Madin, M.E. Herberstein, High-performance spider webs: integrating biomechanics, ecology and behaviour. Journal of the Royal Society Interface 8 (2010) 457–471.

[5] W.M. Masters, H. Markl, Vibration signal transmission in spider orb webs. Science 213 (1981) 363–365.

[6] W.M. Masters, Vibrations in the orb-webs of Nuctenea sclopetaria (Araneidae): I. Transmission through the web. Behavioral ecology and sociobiology 15 (1984) 207–215.

[7] W.M. Masters, Vibrations in the orb-webs of Nuctenea sclopetaria (Araneidae): I. Prey and wind signals and the spider's response threshold. Behavioral ecology and sociobiology 15 (1984) 217–223.

[8] C. Frohlich, R.E. Buskirk, Transmission and attenuation of vibration in orb spider webs. Journal of Theoretical Biology 95 (1982) 13–36.

[9] M.A. Landolfa, F.G. Barth, Vibrations in the orb web of the spider *Nephila clavipes*: cues for discrimination and orientation. Journal of Computational Physiology 179 (1986) 493–508.

[10] B. Mortimer, S.D. Gordon, C. Holland, C.R. Siviour, F. Vollrath, J.F.C. Windmill, The speed of sound in silk: linking material performance to biological function. Advanced Materials 26 (2014) 5179–5183.

[11] F. Vollrath, M. Downes, S. Krackov, Design variability in web geometry of an orb-weaving spider. Physiology & Behavior 62 (1997) 735–743.

[12] C.C Wu, S.J. Blamires, C.L. Wu, I.M. Tso, Wind induces variations in spider web geometry and sticky spiral droplet volume. Journal of Experimental Biology 216 (2013) 3342–3349.

[13] E. Wirth, F.G. Barth, Forces in the spider orb web. Journal of Comparative Physiology A 171 (1992) 359–371.

[14] J. Gosline, M. Lillie, E. Carrington, P. Guerette, C. Ortlepp, K. Savage, Elastic proteins: biological roles and mechanical properties. Philosophical Transactions of the Royal Society B. Biological Sciences 357 (2002) 121–132.

[15] K. Nakata, Attention focusing in a sit-and-wait forager: a spider controls its prey-detection ability in different web sectors by adjusting thread tension. Proceedings of the Royal Society B 277 (2010) 29–33.

[16] F.K. Ko, J. Jovicic, Modeling of mechanical properties and structural design of spider webs. Biomacromolecules 5 (2004) 780–785.

[17] S.W. Cranford, A. Tarakanova, N.M. Pugno, M.J. Buehler, Nonlinear material behaviour of spider silk yields robust webs. Nature 482 (2012) 72–76.

[18] T. Hesselberg, F. Vollrath, The mechanical properties of the non-sticky spiral in *Nephila* orb webs (Araneae, Nephilidae). The Journal of Experimental Biology 215 (2012) 3362–3369.

[19] L.H. Lin, W. Sobek, Structural hierarchy in spider webs and spiderweb-type systems. The Structural Engineer 76 (1998) 59–64.

[20] M.S. Alam, C.H. Jenkins, Damage tolerance in naturally compliant structures. International Journal of Damage Mechanics 14 (2005) 365–383.

[21] A. Tarakanova, M. Buehler, The role of capture spiral silk properties in the diversification of orb webs. Journal of the Royal Society Interface 9 (2012) 3240–3248.

[22] A. Tarakanova, M. Buehler, A materiomics approach to spider silk: protein molecules to webs. Journal of the Minerals, Metals and Materials Society 64 (2012) 214–225.

[23] M.S. Alam, M.A. Wahab, C.H. Jenkins, Mechanics in naturally compliant structures. Mechanics of Materials 39 (2007) 145–160.

[24] N.M. Pugno, S.W. Cranford, M.J. Buehler, Synergical material and structure optimization yields robust spider web anchorages. Small 9 (2013) 2747–2756.

[25] Z. Qin, B.G. Compton, J.A. Lewis, M.J. Buehler, Structural optimization of 3D-printed synthetic spider webs for high strength. Nature Communications (2015) DOI:10.1038/ncomms8038 (7 pages).

[26] R. Zaera, A. Soler, J. Teus, Uncovering changes in spider orb-web topology owing to aerodynamic effects. Journal of the Royal Society Interface 11 (2014) paper 20140484.

[27] A. Soler, R. Zaera, The secondary frame in spider orb webs: the detail that makes the difference. Scientific Reports 6 (2016) DOI:10.1038/srep31265.

[28] B. Mortimer, A. Soler, C.R. Siviour, R. Zaera, F. Vollrath, Tuning the instrument: sonic properties in the spider's web. Journal of the Royal Society Interface 13 (2016) DOI:10.1098/rsif.2016.0341.

[29] Y. Aoyanagi, K. Okumura, Simple model for the mechanics of spider-webs. Physical Review Letters 104 (2010) paper 038102.

[30] Y. Aoyanagi, K. Okumura, Erratum. Physical Review Letters 115 (2015) paper 039903.

[31] H. Tottenham, P.G. Williams, Cable net: continuous systems analysis. Proceedings of the American Society of Civil Engineers 96 (1970) 277–293.

[32] R.S. Rivlin, Plane strain of a net formed by inextensible cords. Journal of Rational Mechanics and Analysis 4 (1955) 951–974.

[33] A.C. Pipkin, Stress analysis for fiber-reinforced materials. Advances in Applied Mechanics 19 (1979) 1–51.

[34] A.C. Pipkin, Energy theorems for infinitesimal plane wrinkling of inextensible networks. IMA Journal of Applied Mathematics 54 (1995) 285-299.

[35] C. Davini, P. Governatori, Nets with hexagonal cell structure. *Journal of Elasticity* 92 (2008) 35-59.

[36] S. Zschokke, Early stages of orb web construction in Araneus diadematus Clerck. Revue Suisse de Zoologie 2 (1996) 709-720.

[37] J. Barros-Neto, An introduction to the theory of distributions, Marcel Dekker, New York, 1973.

[38] R. Carlson, Inverse Sturm-Liouville problems with singularity at zero. Inverse Problems 10 (1994) 851–864.

Table Captions

Table 1. Parameters defining the web geometry for auxiliary and catching spirals.

Table 2. Parameters defining the pre-stress state of the web, after completion of the auxiliary and catching spiral. Values consistent with the results provided by Wirth and Barth [13].

Table 3. Free transverse vibration of the orb-web with the *auxiliary* spiral. First ten nondimensional frequencies for $n = 0$ and $n = 1$.

Table 4. Free transverse vibration of the orb-web with the *auxiliary* spiral. First ten nondimensional frequencies for $n = 2$ and $n = 3$.

Table 5. Free transverse vibration of the orb-web with the *catching* spiral. First 4 nondimensional frequencies for $n = 0$ to $n = 3$. Ω_D^{SL} represents the frequency obtained with the discrete model with masses of spiral silk lumped at the thread intersections. Ω_D^{SRL} represents the frequency obtained with the discrete model with masses of both spiral and radial silk lumped at the thread intersections.

Table 6. Free in-plane vibration of the orb-web with the *catching* spiral. First ten nondimensional frequencies.

Figure Captions

Figure 1. Referential placement in polar coordinate representation on covariant basis.

Figure 2. Actual configuration, covariant and contravariant basis, and internal force assumption.

Figure 3. Radial fiber density in referential configuration.

Figure 4. Sketch of the discrete models for the web with *auxiliary* and *catching* spirals.

Figure 5. Nondimensional transverse displacement vs. nondimensional radial position. Web with *auxiliary* spiral submitted to out-of-plane static point ($\bar{P} = 0.1$) and uniformly distributed ($\bar{p} = 0.1$) loads.

Figure 6. Nondimensional transverse displacement vs. nondimensional radial position. Web with *catching* spiral submitted to out-of-plane static point ($\bar{P} = 0.1$) and uniformly distributed ($\bar{p} = 0.1$) loads.

Figure 7. Discrete model of the orb-web with the *auxiliary* spiral. First two transverse vibration modes for $n = 0$ to $n = 3$.

Figure 8. Continuum model of the orb-web with the *auxiliary* spiral. First two transverse vibration modes for $n = 0$ to $n = 3$.

Figure 9. Web with *auxiliary* spiral. Transverse vibration modes 1 to 4 for $n = 0$ (normalized for $max|\tilde{u}| = 1$). Comparison between continuum and discrete models.

Figure 10. Web with *catching* spiral. Transverse vibration modes 1 to 4 for $n = 0$ (normalized for $max|\tilde{u}| = 1$). Comparison between continuum and discrete models. Differences between results from the discrete model with spiral mass lumped, and from the discrete model with both spiral and radial mass lumped, are visually imperceptible.

Figure 11. Mode shapes 3 and 4 corresponding to $n = 0$ for the orb-web with the *catching* spiral, calculated with the continuum and discrete (uniform mass distribution and lumped mass) models. Differences between results from the discrete model with spiral mass lumped, and from the discrete model with both spiral and radial mass lumped, are visually imperceptible.

Figure 12. In-plane vibration modes 1 to 4 (normalized for $max|\tilde{u}| = 1$). Comparison between continuum and discrete models.

Table 1: Parameters defining the web geometry for auxiliary and catching spirals.

Parameter	Auxiliary	Catching
R	0.12 m	0.12 m
C_ϑ	100 m^{-1}	308 m^{-1}
C_ρ	$32/(2\pi)$	$32/(2\pi)$
ϕ_ϑ	2.3 μm	2.3 μm
ϕ_ρ	3.5 μm	3.5 μm
ϱ_S	1098 $\mathrm{kg/m}^3$	1098 $\mathrm{kg/m}^3$
E_ρ	11.0 GPa	11.0 GPa
E_ϑ	50.0 MPa	

Table 2: Parameters defining the pre-stress state of the web, after completion of the auxiliary and catching spiral. Values consistent with the results provided by Wirth and Barth [13].

Parameter	Auxiliary	Catching
$\widehat{T}$	14	125 μN
$k\xi$	32.2 m^{-1}	-
$\mathcal{T}$	-	10 μN

Table 3: Free transverse vibration of the orb-web with the *auxiliary* spiral. First ten nondimensional frequencies for $n = 0$ and $n = 1$.

n	Mode	Discrete Ω_D	Continuum Ω_C	Relative $\frac{\Omega_D - \Omega_C}{\Omega_D}$ (%)
0	1	0.711	0.707	0.558
	2	1.598	1.592	0.378
	3	2.533	2.531	0.070
	4	3.482	3.496	-0.386
	5	4.433	4.478	-1.013
	6	5.366	5.476	-2.041
	7	6.257	6.490	-3.710
	8	7.113	7.521	-5.731
	9	8.217	8.571	-4.310
	10	9.233	9.641	-4.425
1	1	1.462	1.453	0.638
	2	2.296	2.287	0.394
	3	3.188	3.188	0.002
	4	4.105	4.128	-0.573
	5	5.027	5.095	-1.354
	6	5.954	6.084	-2.185
	7	6.925	7.094	-2.445
	8	7.772	8.124	-4.538
	9	8.413	9.177	-9.078
	10	9.829	10.251	-4.293

Table 4: Free transverse vibration of the orb-web with the *auxiliary* spiral. First ten nondimensional frequencies for $n = 2$ and $n = 3$.

n	Mode	Discrete Ω_D	Continuum Ω_C	Relative $\frac{\Omega_D - \Omega_C}{\Omega_D}$ (%)
2	1	2.193	2.195	-0.120
	2	2.901	2.909	-0.299
	3	3.680	3.705	-0.684
	4	4.504	4.563	-1.317
	5	5.348	5.468	-2.245
	6	6.202	6.408	-3.316
	7	7.128	7.379	-3.524
	8	7.982	8.378	-4.969
	9	8.680	9.404	-8.348
	10	10.061	10.457	-3.940
3	1	2.989	3.037	-1.603
	2	3.628	3.691	-1.736
	3	4.316	4.409	-2.159
	4	5.041	5.190	-2.943
	5	5.782	6.025	-4.203
	6	6.555	6.907	-5.369
	7	7.440	7.828	-5.209
	8	8.342	8.784	-5.297
	9	9.104	9.773	-7.349
	10	10.414	10.794	-3.646

Table 5: Free transverse vibration of the orb-web with the *catching* spiral. First 4 nondimensional frequencies for $n = 0$ to $n = 3$. Ω_D^{SL} represents the frequency obtained with the discrete model with masses of spiral silk lumped at the thread intersections. Ω_D^{SRL} represents the frequency obtained with the discrete model with masses of both spiral and radial silk lumped at the thread intersections.

n	Mode	Discrete model Ω_D	Continuum model Ω_C	Relative error $\frac{\Omega_D-\Omega_C}{\Omega_D}$ (%)	Relative error $\frac{\Omega_D^{SL}-\Omega_C}{\Omega_D^{SL}}$ (%)	Relative error $\frac{\Omega_D^{SRL}-\Omega_C}{\Omega_D^{SRL}}$ (%)
0	1	0.213	0.213	-0.119	0.048	0.017
	2	0.546	0.561	-2.769	-0.027	0.049
	3	0.843	0.920	-9.170	-0.188	-0.327
	4	1.044	1.282	-22.862	-0.432	-0.685
1	1	0.370	0.373	-0.889	0.012	-0.024
	2	0.699	0.734	-5.126	-0.106	-0.200
	3	0.958	1.097	-14.556	-0.208	-0.497
	4	1.092	1.463	-34.019	-0.595	-0.916
2	1	0.418	0.421	-0.819	-0.128	-0.162
	2	0.734	0.772	-5.219	-0.167	-0.258
	3	0.980	1.129	-15.119	-0.343	-0.530
	4	1.098	1.490	-35.652	-0.617	-0.933
3	1	0.480	0.483	-0.828	-0.532	-0.566
	2	0.784	0.827	-5.488	-0.397	-0.484
	3	1.013	1.176	-16.221	-0.487	-0.667
	4	1.107	1.532	-38.474	-0.714	-1.029

Table 6: Free in-plane vibration of the orb-web with the *catching* spiral. First ten nondimensional frequencies.

Mode	Discrete model Ω_D	Continuum model Ω_C	Relative difference $\frac{\Omega_D - \Omega_C}{\Omega_D}$ (%)
1	0.310	0.310	-0.079
2	0.629	0.630	-0.209
3	0.947	0.951	-0.425
4	1.263	1.272	-0.732
5	1.578	1.596	-1.131
6	1.891	1.922	-1.623
7	2.203	2.252	-2.208
8	2.513	2.585	-2.889
9	2.820	2.923	-3.669
10	3.124	3.266	-4.551

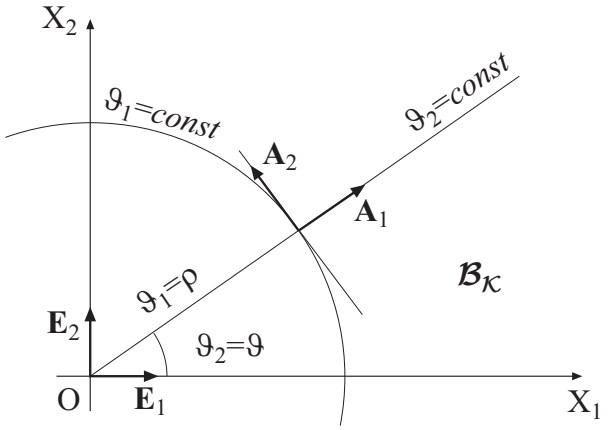

Figure 1: Referential placement in polar coordinate representation on covariant basis.

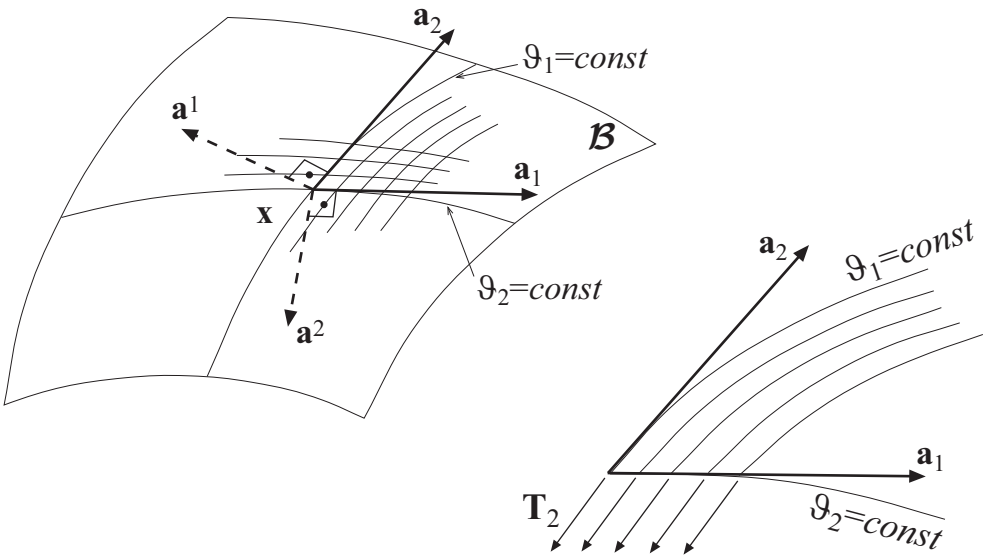

Figure 2: Actual configuration, covariant and contravariant basis, and internal force assumption.

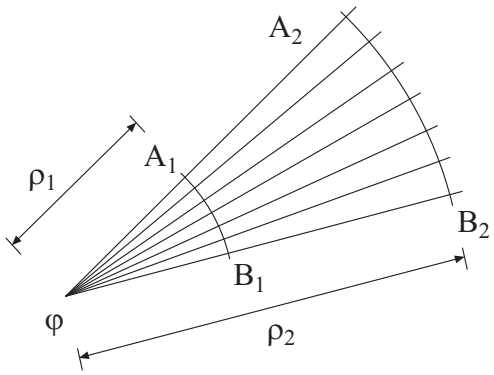

Figure 3: Radial fiber density in referential configuration.

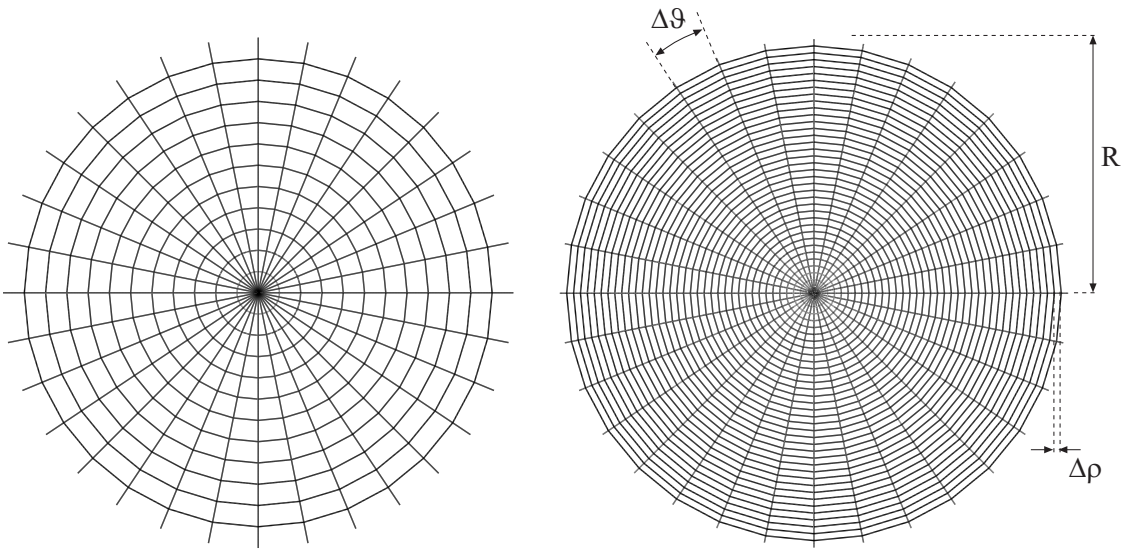

Figure 4: Sketch of the discrete models for the web with *auxiliary* and *catching* spirals.

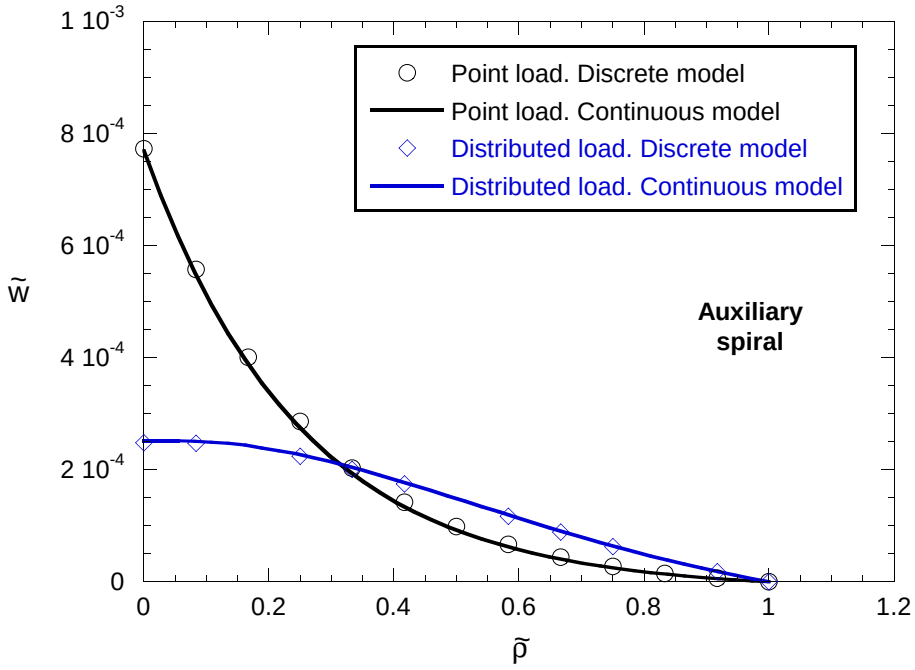

Figure 5: Nondimensional transverse displacement vs. nondimensional radial position. Web with *auxiliary* spiral submitted to out-of-plane static point ($\bar{P} = 0.1$) and uniformly distributed ($\bar{p} = 0.1$) loads.

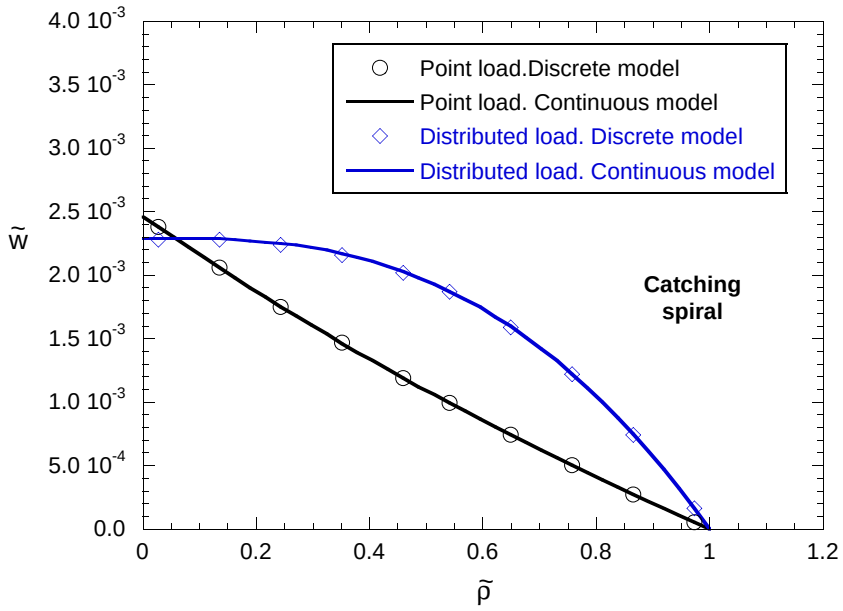

Figure 6: Nondimensional transverse displacement vs. nondimensional radial position. Web with *catching* spiral submitted to out-of-plane static point ($\bar{P} = 0.1$) and uniformly distributed ($\bar{p} = 0.1$) loads.

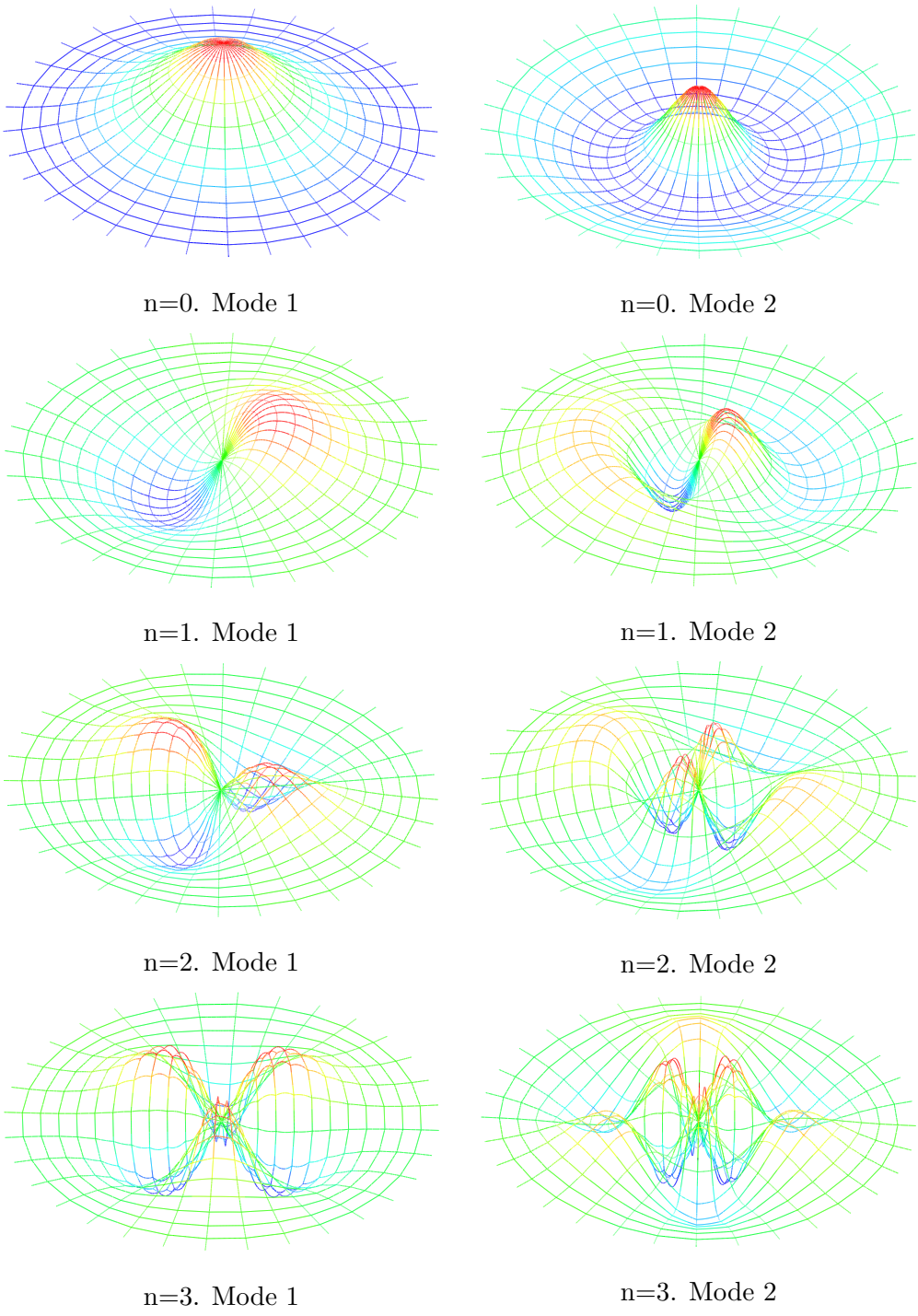

Figure 7: Discrete model of the orb-web with the *auxiliary* spiral. First two transverse vibration modes for $n = 0$ to $n = 3$.

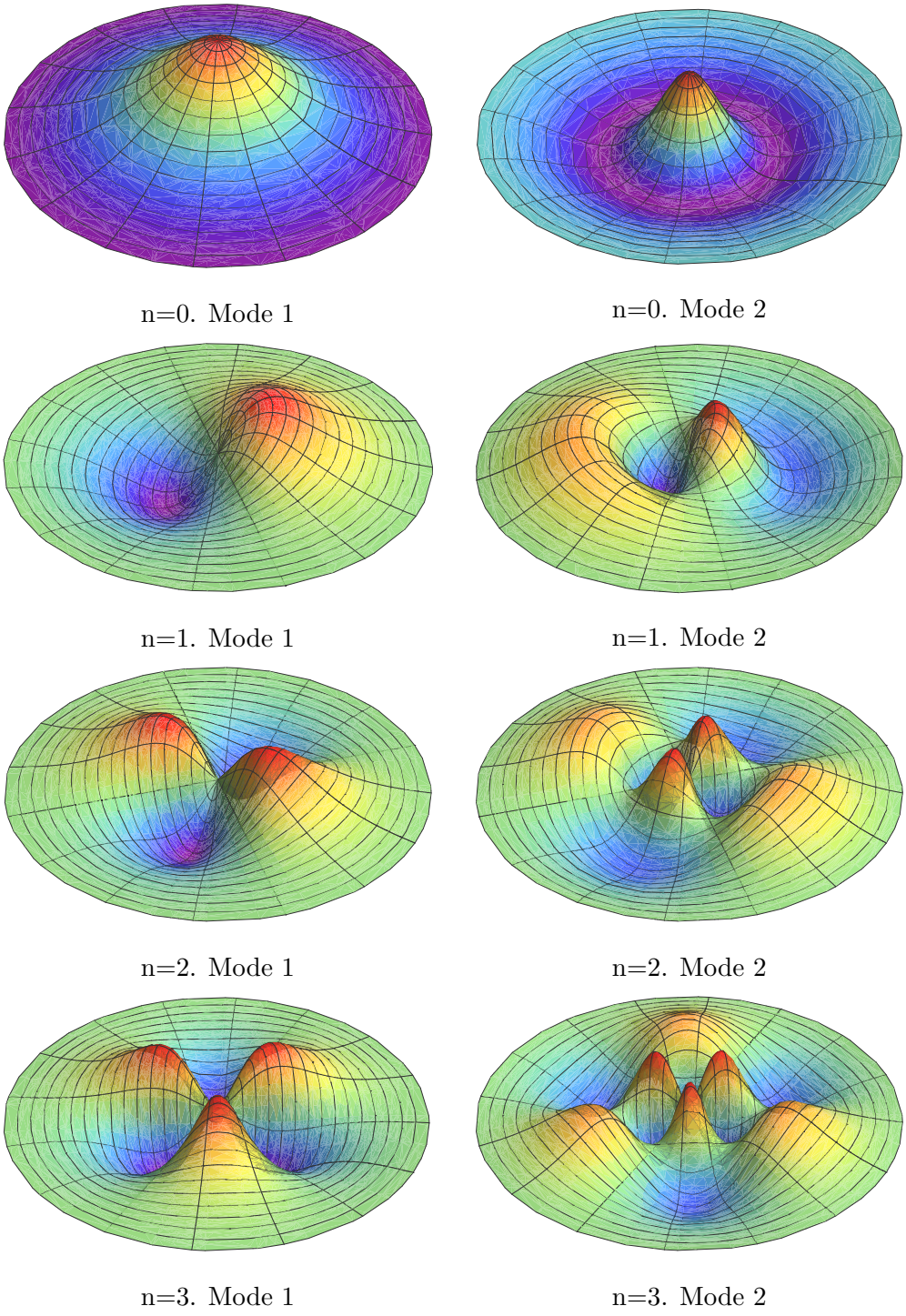

Figure 8: Continuum model of the orb-web with the *auxiliary* spiral. First two transverse vibration modes for $n = 0$ to $n = 3$.

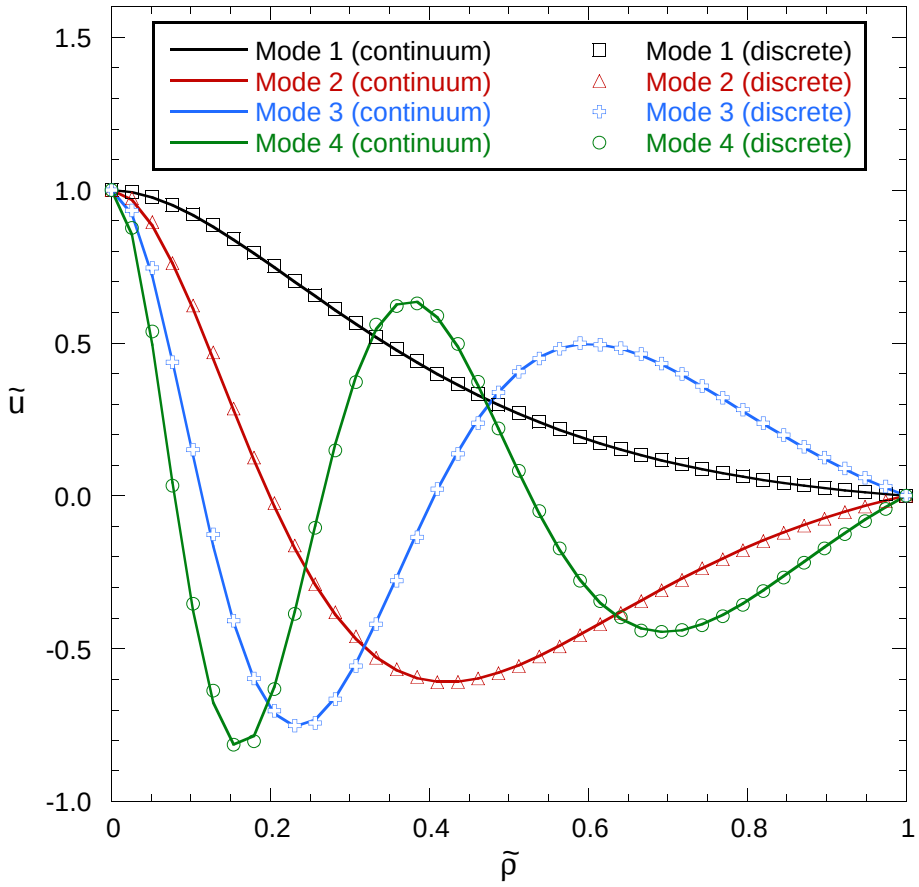

Figure 9: Web with *auxiliary* spiral. Transverse vibration modes 1 to 4 for $n = 0$ (normalized for $max|\tilde{u}| = 1$). Comparison between continuum and discrete models.

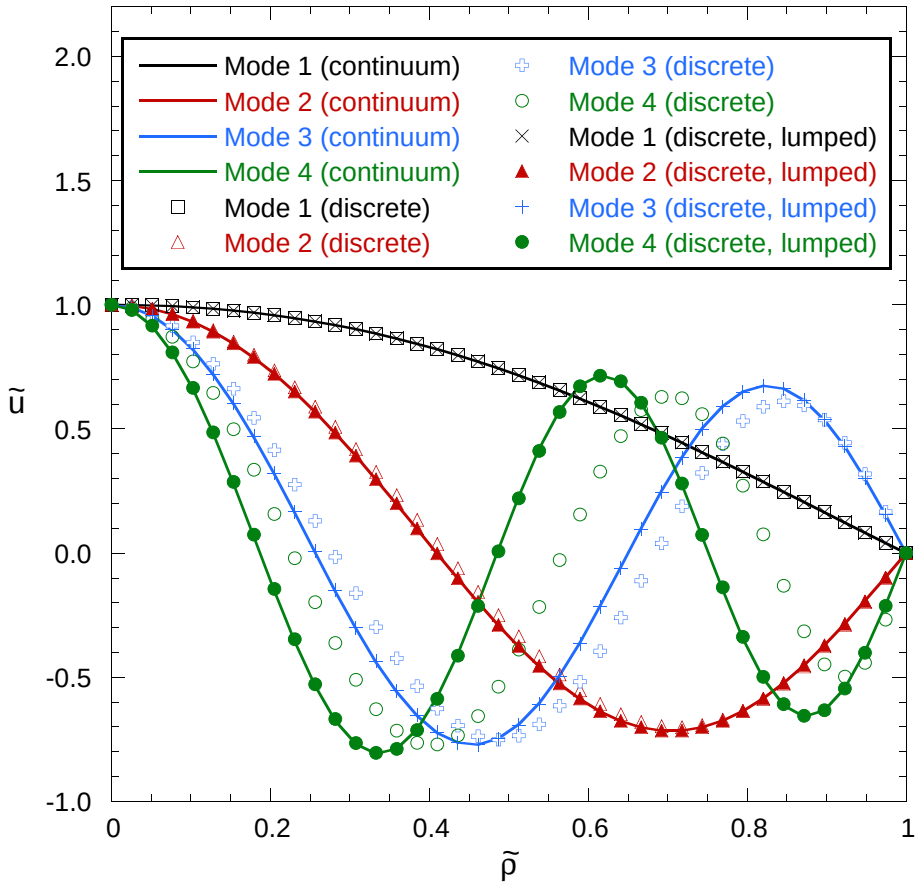

Figure 10: Web with *catching* spiral. Transverse vibration modes 1 to 4 for $n = 0$ (normalized for $max|\tilde{u}| = 1$). Comparison between continuum and discrete models. Differences between results from the discrete model with spiral mass lumped, and from the discrete model with both spiral and radial mass lumped, are visually imperceptible.

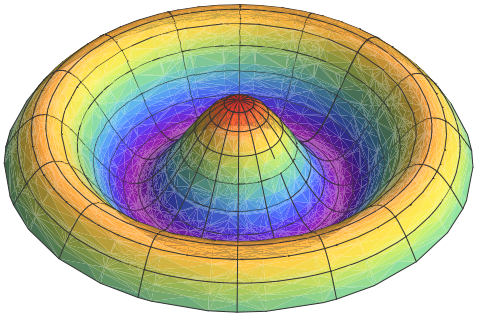

Mode 3. Continuum model

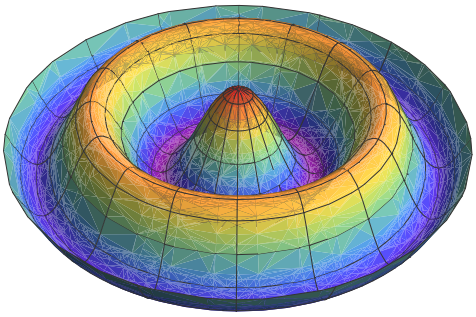

Mode 4. Continuum model

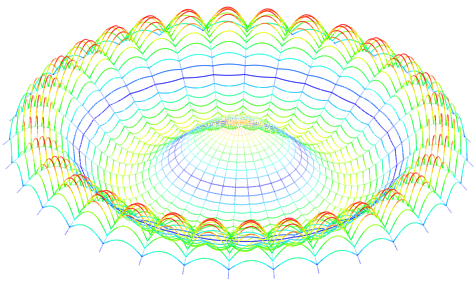

Mode 3. Discrete model

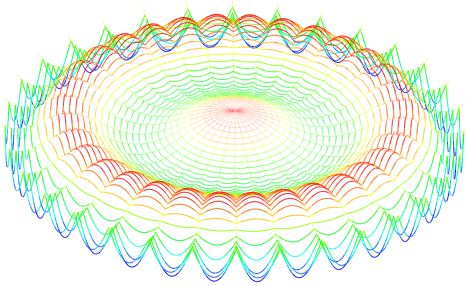

Mode 4. Discrete model

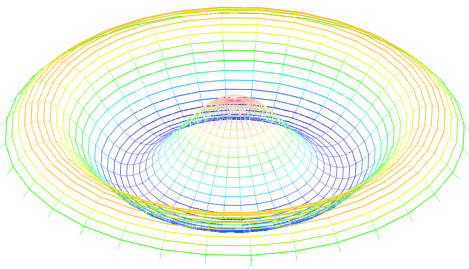

Mode 3. Discrete model (lumped)

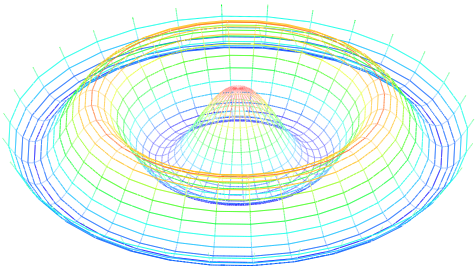

Mode 4. Discrete model (lumped)

Figure 11: Mode shapes 3 and 4 corresponding to $n = 0$ for the orb-web with the *catching* spiral, calculated with the continuum and discrete (uniform mass distribution and lumped mass) models. Differences between results from the discrete model with spiral mass lumped, and from the discrete model with both spiral and radial mass lumped, are visually imperceptible.

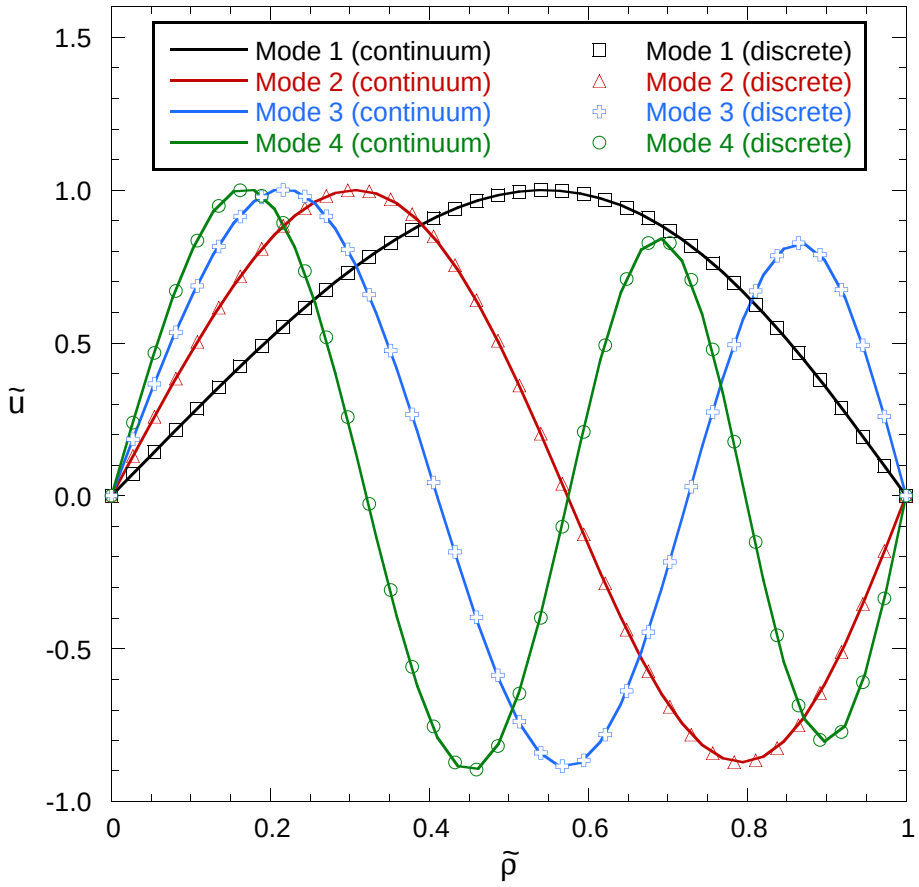

Figure 12: In-plane vibration modes 1 to 4 (normalized for $max|\tilde{u}| = 1$). Comparison between continuum and discrete models.